NEUROSCIENCE

Neuronal potassium channel activity triggers initiation of mRNA translation through binding of translation regulators

Taylor J. Malone[1,2]†, Jing Wu[1]†, Yalan Zhang[1]†, Pawel Licznerski[3], Rongmin Chen[3], Sheikh Nahiyan[1], Maysam Pedram[1], Elizabeth A. Jonas[3,4], Leonard K. Kaczmarek[1,2]*

Neuronal activity stimulates mRNA translation crucial for learning and development, but the mechanism linking translation to neuronal activity is not understood. In humans, learning and memory are severely disrupted by mutations in the potassium channel Slack (KCNT1, Slo2.2). We find that pharmacological stimulation of this channel and a constitutively active Slack mutation stimulate mRNA translation of a reporter for β-actin mRNA in cell lines and increases the synthesis of β-actin in the neurites of cortical neurons. Moreover, channel activation promotes the binding of two key mRNA translation regulators, FMRP (fragile X mental retardation protein) and CYFIP1 (cytoplasmic FMR1–interacting protein 1), to the channel itself, releasing both from eIF4E (eukaryotic initiation factor 4E), where they normally inhibit initiation of translation. This interaction provides a molecular mechanism for Slack activity–dependent regulation of translation and suggests that the effects of Slack mutations on this process may explain the severe intellectual disabilities associated with these mutations.

INTRODUCTION

The Slack channel (sequence like a calcium-activated potassium channel, also termed $K_{Na}1.1$, KCNT1, or Slo2.2) is a sodium-activated potassium channel (K_{Na} channel) that can be activated by Na^+ influx through various pathways, including the voltage-dependent Na^+ (Na_V) channels, nonselective HCN cation channels, or AMPA receptors (*1*–*3*). Slack is predominantly expressed in neurons of the central nervous system where it regulates neuronal excitability (*1*, *2*, *4*–*6*). In the past 10 years, gain-of-function mutations in the Slack channel have been identified in patients with several distinct early onset epilepsy disorders (*7*–*9*), all of which are also associated with severe intellectual disability (*10*). Slack was also the first of several ion channels shown to interact directly with the mRNA-binding protein fragile X mental retardation protein (FMRP) (*11*, *12*). Other FMRP-binding channels include Kv1.2, Kv4.3, BK, SK2, Cav2.2, and Cav3.1 (*13*–*19*). In all cases, the interaction of FMRP alters some aspects of channel activity. For example, FMRP binding to Slack increases the Slack open probability and current and modulates action potential shape (*11*, *12*).

In neurons, FMRP regulates both the trafficking and activity of its mRNA targets, controlling local translation via several different mechanisms (*20*–*23*). Slack channels also bind another regulator of mRNA translation, CYFIP1 [cytoplasmic FMR1–interacting protein 1, also known as a eukaryotic initiation factor 4E (eIF4E)–binding protein (4E-BP)] (*24*). Among its functions, FMRP controls initiation of translation by forming a complex with CYFIP1 (*25*). The FMRP/CYFIP1 complex binds the initiation factor eIF4E, suppressing the first step in protein synthesis (*25*–*29*). Upon neuronal stimulation, the FMRP/CYFIP1 complex dissociates from eIF4E, releasing FMRP target mRNAs for translation (*25*).

The regulation of ion channel activity, including that of Slack, by FMRP has previously been considered a noncanonical function of FMRP, distinct from its role in the regulation of translation. It is possible, however, that Slack could reciprocally regulate the functions of FMRP in translation. This is supported by the finding that Slack channels have been found to be required for protein synthesis–dependent changes in the excitability of neurons in *Aplysia* (*12*). We have now found that pharmacological stimulation of the wild-type Slack channel promotes translation in both cell lines and neurons and that a disease-causing mutation in the C terminus of Slack (*Slack-R455H*), which constitutively activates the channel, results in constitutive activation of translation, an effect that requires the untranslated region (UTR) of the mRNA. Furthermore, we demonstrate that activation of Slack channels triggers the redistribution of FMRP and CYFIP1, increasing their binding to the channel complex and releasing them from eIF4E. Last, suppressing FMRP and CYFIP1 expression abolishes the ability of the channel to stimulate translation. The link between channel activity and stimulation of protein synthesis, as well as its dysregulation by mutations, is likely to play a key role in the intellectual disability observed in patients with Slack mutations.

RESULTS

Gain-of-function *Slack-R455H* mutation increases protein expression of a β-actin reporter construct

To measure the active translation of ribosome-associated RNAs, we used a reporter construct, dendra2$_{actin}$, which contains the coding region of the fluorescent protein dendra2 flanked by the β-actin 5′UTR and 3′UTR in a pCS2 vector (Fig. 1A). This reporter was selected because β-actin mRNA is a known binding target of FMRP (*30*) and β-actin is rapidly translated in response to neuronal stimulation (*31*). Dendra2 fluorescence can be irreversibly photoconverted to red fluorescence or photobleached using a 405- or 488-nm laser, respectively

[1]Department of Pharmacology, Yale University School of Medicine, New Haven, CT 06520, USA. [2]Department of Cellular and Molecular Physiology, Yale University School of Medicine, New Haven, CT 06520, USA. [3]Department of Internal Medicine, Section of Endocrinology, Yale University School of Medicine, New Haven, CT 06520, USA. [4]Department of Neuroscience, Yale University School of Medicine, New Haven, CT 06520, USA.
*Corresponding author. Email: leonard.kaczmarek@yale.edu
†These authors contributed equally to this work.

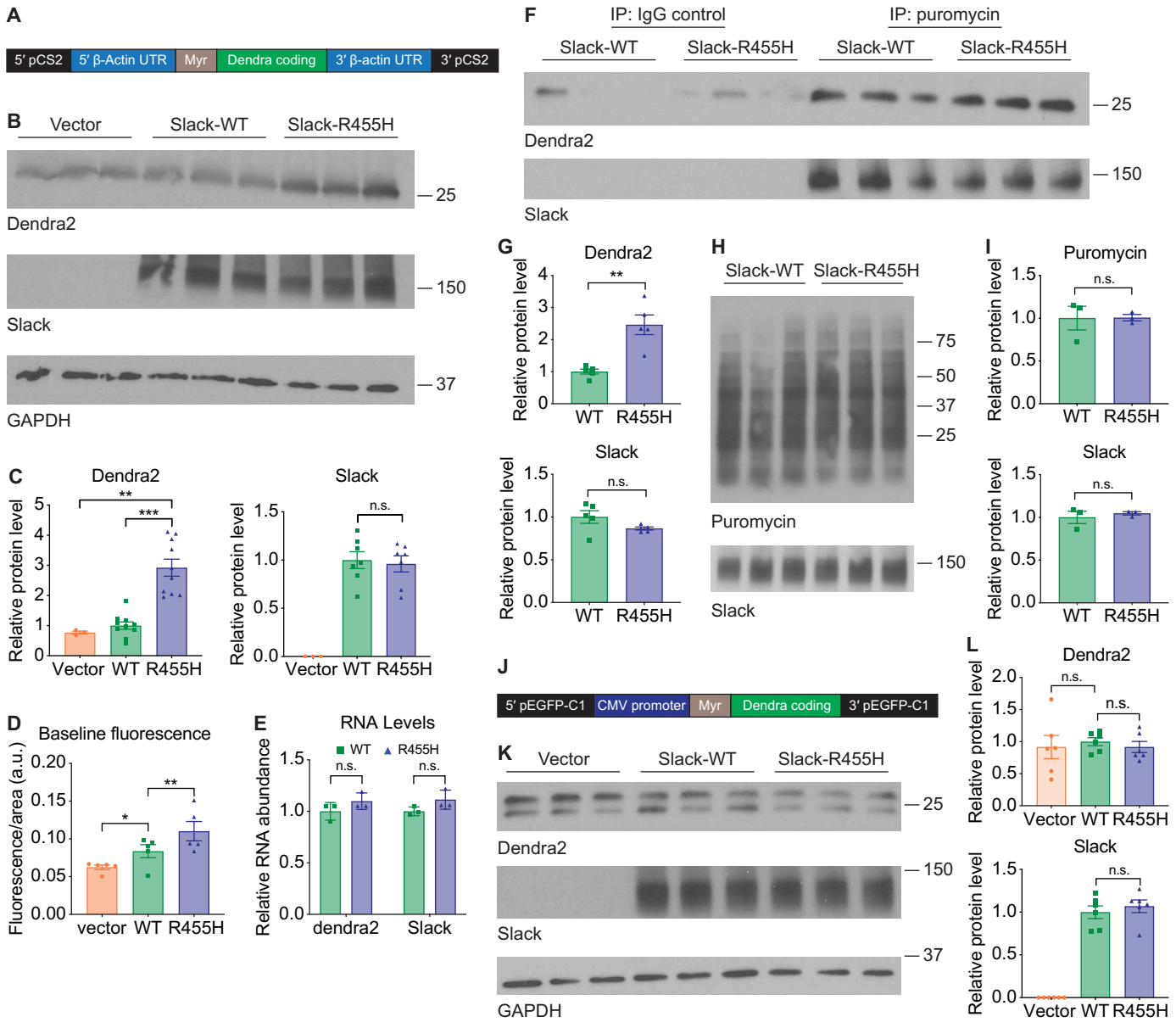

Fig. 1. *Slack-R455H* mutation increases translation of β-actin reporter construct. (**A**) Schematic of β-actin translation reporter construct: Fluorescent dendra2 protein flanked by 5′UTR and 3′UTR of β-actin contains nonfunctional myristylation (myr) tag. (**B** and **C**) Protein expression of dendra2 and Slack ($n = 3$ to 10 replicates), and (**D**) baseline fluorescence intensity of the dendra2$_{actin}$ reporter [$n = 5$ plates, six FOV per plate, 3 to 22 cells per FOV, two-way analysis of variance (ANOVA) with post hoc comparisons] in human embryonic kidney (HEK) cells 24 hours after co-transfection of dendra2$_{actin}$ with vector control, rat wild-type Slack (*Slack-WT*, WT), or *Slack-R455H* (R455H). a.u., arbitrary units. (**E**) qPCR of dendra2 and Slack mRNA levels ($n = 3$ replicates) and (**F** and **G**) actively translating protein of dendra2 and Slack using puromycin treatment and puromycin antibody IP ($n = 5$ replicates) 24 hours after co-transfection of dendra2$_{actin}$ with *Slack-WT* or *Slack-R455H*. (**H** and **I**) Global translation levels ($n = 3$ replicates) after puromycin treatment 24 hours after transfection with *Slack-WT* or *Slack-R455H*. (**J**) Schematic of subcloned dendra2 reporter construct inserted into pEGFP-C1 vector without β-actin UTR. (**K** and **L**) Protein expression of dendra2 and Slack ($n = 6$ replicates) in HEK cells 24 hours after co-transfection of dendra2-C1 with vector control, *Slack-WT*, or *Slack-R455H*. [(C), (I), and (L)] Data are first normalized by glyceraldehyde-3-phosphate dehydrogenase (GAPDH) [(C) and (L)] or Slack (I) levels and then to Slack-WT level [(C), (G), (I), and (L)]. (E) *Gapdh* was used as the housekeeping gene. (G) Data are normalized to Slack-WT level. Comparisons for all panels except D used unpaired *t* test. Data are expressed as means ± SEM. *$P < 0.05$; **$P < 0.01$; ***$P < 0.001$. See data S2 for exact *P* values. n.s., not significant.

(*32*, *33*). This construct contains a nonfunctional myristylation tag (myr) that would normally target the protein to the cell membrane. This nonfunctional tag was removed for a subset of experiments described later. We compared the translation of this reporter in cells and neurons expressing either wild-type Slack or the gain-of-function mutant *Slack-R455H*. The *Slack-R455H* mutation in mice and rats corresponds to the human mutation *Slack-R474H*, which causes epilepsy of infancy with migrating focal seizures (EIMFS) with severe intellectual disability and results in one the greatest increases in K^+ current among Slack mutations (*34*, *35*). As is the case with humans, heterozygote mice bearing one copy of this mutation have seizures and persistent interictal spikes but homozygous *Slack-R455H* mice

do not survive birth (*35*). For simplicity, the heterozygotes are termed *Slack-R455H* mice in this study.

We first compared levels of dendra2$_{actin}$ in human embryonic kidney (HEK) cells transiently co-expressing either wild-type rat *Slack* or *Slack-R455H*. While wild-type Slack had no effect relative to an empty vector, *Slack-R455H* significantly increased levels of dendra2 protein detected on Western blots (Fig. 1, B and C). Slack protein levels themselves were unchanged between wild-type Slack and *Slack-R455H* expressing cells, ruling out preferential translation of dendra2 due to a poorly expressed *Slack-R455H* construct (Fig. 1, B and C). We also measured baseline dendra2 fluorescence levels, as increased reporter expression should lead to increased fluorescence. Dendra2 baseline fluorescence was significantly increased when co-expressed with wild-type Slack compared to an empty vector and further increased when expressed with *Slack-R455H* (Fig. 1D). The observed difference between vector and wild-type Slack conditions only in fluorescence levels is likely due to differences in sensitivity between the two assays. The fluorescence assay examines individual transfected cells, while the Western blotting measures bulk protein from both transfected and untransfected cells.

These results demonstrate that the *Slack-R455H* mutation increases the expression of the dendra2$_{actin}$ reporter. To test for possible effects of Slack on transcription, real-time quantitative polymerase chain reaction (qPCR) was performed to examine mRNA levels for dendra2$_{actin}$ and Slack. No differences in mRNA levels were observed when dendra2$_{actin}$ was co-transfected with wild-type Slack or *Slack-R455H*, suggesting that changes in transcription do not contribute to *Slack-R455H*-mediated regulation of dendra2$_{actin}$ protein levels (Fig. 1E).

Slack-R455H mutation specifically increases mRNA translation of the β-actin reporter construct

We next examined whether the *Slack-R455H* mutation alters the translation of dendra2$_{actin}$ mRNA using a puromycin incorporation assay. Puromycin is a mild translation inhibitor that covalently binds to the nascent peptide strand at the ribosome, causing its release (*36*). Incubating cells with puromycin before protein extraction allows the labeling of proteins that are being actively synthesized and can be used to measure global translation levels. We combined this technique with co-immunoprecipitation (co-IP) to detect the translating population of specific proteins. We found that levels of actively translating dendra2 were increased when expressed with *Slack-R455H* compared to wild-type Slack (Fig. 1, F and G). Again, there were no statistically significant changes in the rate of incorporation of puromycin into Slack. The increase in dendra2$_{actin}$ translation without a change in Slack levels suggests that *Slack-R455H* may specifically regulate dendra2$_{actin}$ translation without affecting global translation. Alternatively, Slack translation could be specifically protected from regulation.

To assess global translation levels, we performed a traditional puromycin incorporation assay in HEK cells transfected with either wild-type Slack or *Slack-R455H*, without co-transfection of the dendra2$_{actin}$ reporter. The expression of *Slack-R455H* had no effect on global translation levels compared to wild-type Slack (Fig. 1, H and I). While this result does not rule out the possibility that Slack regulates additional targets, it suggests that its regulation is limited in scope.

The β-actin UTRs are the target of *Slack-R455H* regulation

The specificity of the effect of *Slack-R455H* in stimulating translation of dendra2$_{actin}$ could, in theory, reside in sequences in either the β-actin UTR or the dendra2 coding region. To determine whether regulation by *Slack-R455H* requires the β-actin UTR, we generated an alternate dendra2 construct (dendra2-C1), in which the coding region of dendra2 was inserted into an alternate vector (pEGFP-C1), which lacks the β-actin UTR (Fig. 1J). We found no difference in dendra2 protein levels when dendra2-C1 was co-expressed with an empty vector, wild-type Slack, or *Slack-R455H* (Fig. 1, K and L), confirming that the β-actin UTR is a target of Slack regulation.

Activation of wild-type Slack channels stimulates translation of the β-actin reporter construct

To further test the effects of Slack activation on translation, we used the fluorescence recovery after photobleaching (FRAP) technique to monitor dendra2$_{actin}$ fluorescence in real time in HEK cells co-transfected with the dendra2$_{actin}$ reporter and either wild-type Slack or an empty vector as a negative control. These cells were subjected to treatment with either the Slack activator niclosamide (10 μM), a compound known to activate both wild-type and EIMFS mutant Slack channels (*24*), or with dimethyl sulfoxide (DMSO; vehicle) for 30 min. Dendra2 is irreversibly photoconverted to red fluorescence or irreversibly photobleached by 405- and 488-nm light, respectively (*32*, *33*). Because the rate of maturation of the dendra2 protein is fast (*32*), the rate of fluorescence recovery after the photobleaching of an entire cell provides a measure of newly synthesized dendra2 protein (Fig. 2A). Although some previous studies with dendra2 have used photoconversion rather than photobleaching for this purpose (*37*, *38*), we found in preliminary experiments that photobleaching caused less cytotoxic damage to the cells while still allowing sufficient depletion of green fluorescence to observe recovery.

The time course of fluorescence recovery of dendra2$_{actin}$ was determined using a two-photon microscope with automated software that obtains baseline images, identifies and photobleaches cells by 50%, and then obtains post-bleach images at 10-min intervals. We compared the time courses of recovery in the presence or absence of the Slack channel activator niclosamide. In the absence of niclosamide, wild-type Slack had no effect on fluorescence recovery of dendra2$_{actin}$ (Fig. 2, B and C). In the presence of niclosamide, however, the rate of fluorescence recovery was greatly increased relative to negative controls. Niclosamide caused a slight increase in fluorescence in negative controls relative to DMSO, likely due to off-target effects, but these changes were much smaller than seen in the presence of wild-type Slack.

To determine whether the ability of Slack channel activation to stimulate synthesis of the reporter is conserved in human Slack channels, we repeated the above experiment using HEK cells stably expressing the wild-type human Slack channel (*hSlack-WT*). These cells were transiently transfected with dendra2$_{actin}$. HEK cells not expressing the channel were used as the negative control. As with the rat channel, *hSlack-WT* had no effect on dendra2$_{actin}$ fluorescence recovery in the absence of niclosamide, but the rate of recovery was markedly stimulated by the channel activator (Fig. 2, D and E). Together, these data indicate that pharmacological activation of both rat and human Slack channels increases translation of the dendra2$_{actin}$ reporter.

To determine whether K^+ flux through Slack channels is required for stimulation of dendra2$_{actin}$ reporter synthesis, we used quinidine, a nonspecific channel pore blocker (*39*, *40*) that inhibits Slack channel–mediated currents (*41*). We carried out FRAP experiments in HEK cells expressing *hSlack-WT*, treated with DMSO, niclosamide,

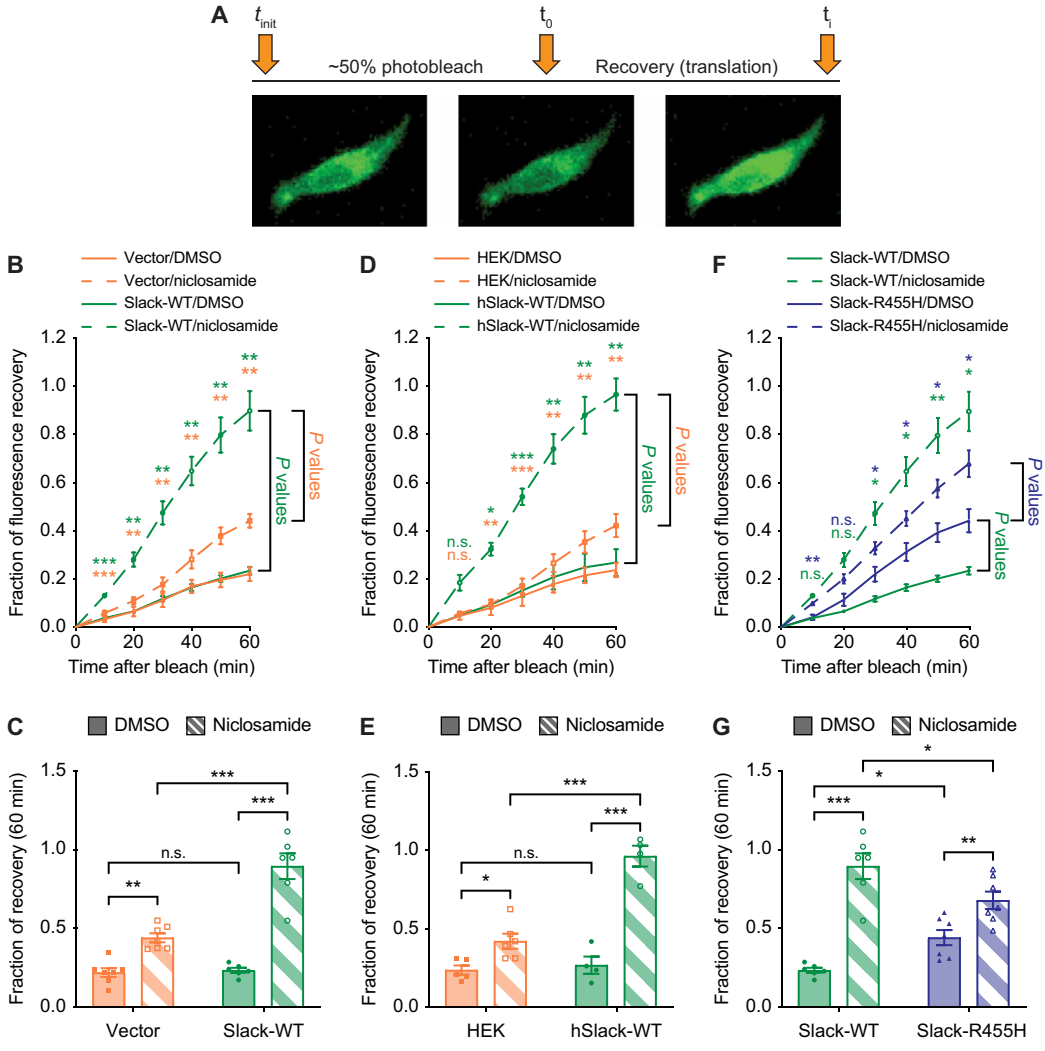

Fig. 2. Slack activation increases translation of β-actin reporter construct. (**A**) Top: Schematic of FRAP experiment protocol. Bottom: Example cell from FRAP experiments (left, pre-photobleaching; center, post-photobleaching; right, post-recovery). (**B** to **G**) FRAP experiments with or without niclosamide (10 μM, 30 min) in HEK cells ($n = 4$ to 8 plates, 13 to 53 cells per plate). [(B) and (C)] Vector control or rat *Slack-WT* were co-transfected with dendra2$_{actin}$. [(D) and (E)] Only dendra2$_{actin}$ was transfected into stable human Slack cells (*hSlack-WT*) or untransfected control cells. [(F) and (G)] Rat *Slack-WT* or *Slack-R455H* were co-transfected with dendra2$_{actin}$. [(B), (D), and (F)] FRAP time course. *P* values represent differences between the groups indicated, two-way repeated-measures ANOVA with post hoc comparisons with Holm-Šídák correction. [(C), (E), and (G)] Bar graph of 60-min recovery time point, ordinary two-way ANOVA with post hoc comparisons. Data are expressed as means ± SEM. $*P < 0.05$; $**P < 0.01$; $***P < 0.001$. See data S2 for exact *P* values. WT, wild type.

or niclosamide and quinidine. We found that, compared to niclosamide alone, co-treatment with quinidine blocked the increase in dendra2$_{actin}$ fluorescence recovery produced by the activator (fig. S1, A and B). While this suggests that K^+ flux through the Slack channel pore may be required for activation of translation, quinidine is a nonspecific channel blocker with potential off-target effects (*39*, *40*). Definitive conclusions will require both the development of more selective pore blockers and the use of genetically engineered nonconducting Slack mutants to distinguish between conductance-dependent and conductance-independent mechanisms.

We next tested whether stimulation of dendra2$_{actin}$ reporter synthesis is simply a consequence of increased K^+ conductance. We compared the effects of Slack with those of the structurally related BK ($K_{Ca}1.1$, KCNMA1, and Slo1) potassium channel. A Chinese Hamster Ovary (CHO) cell line that stably expresses the BK channel was transiently co-transfected with the dendra2$_{actin}$ reporter. Treatment of these cells with the well-characterized BK channel activator NS1619 (*42*) had no statistically significant effect on the rate of FRAP (fig. S1, C and D), suggesting that the increases in translation produced by Slack channels do not result simply from elevated K^+ flux.

Slack-R455H mutation constitutively stimulates translation of the β-actin reporter construct

We next carried out similar FRAP experiments to assess the impact of the *Slack-R455H* mutant on the time course of fluorescence recovery of dendra2$_{actin}$. For this, HEK cells were co-transfected with the dendra2$_{actin}$ reporter and either *Slack-R455H* or wild-type Slack. Consistent with the results of the biochemical experiments in Fig. 1, the presence of the mutant channel significantly increased the rate of fluorescence recovery compared to wild-type Slack, even in the

absence of a channel activator (Fig. 2, F and G). Previous work has shown that some disease-causing mutant Slack channels can still be further activated by niclosamide (*24*). Here, we found that treatment of cells expressing *Slack-R455H* with niclosamide did result in a further increase in the rate of fluorescence recovery (Fig. 2, F and G). Although the degree of stimulation induced by niclosamide appeared slightly reduced relative to wild-type Slack, this is likely due to the higher baseline fluorescence level induced by *Slack-R455H*, as the absolute increase in fluorescence in the presence of niclosamide was not significantly different between wild-type Slack and *Slack-R455H* (fig. S1, E and F).

Endogenous neuronal Slack channels regulate β-actin translation

To determine whether the regulation of translation by Slack channels that we characterized in HEK cells also occurs in neurons, we first carried out similar FRAP experiments using primary cortical neurons from wild-type mice, which express Slack protein endogenously (*5*). Control experiments were carried out using cortical neurons isolated from Slack knockout ($Slack^{-/-}$) mice (*35*, *43*, *44*). Neurons were transiently transfected with dendra2$_{actin}$ as in the experiments with HEK cells, but bleaching and recovery were monitored using manual epifluorescence microscopy and with a single recovery time point. As in HEK cells, the addition of the Slack activator niclosamide in wild-type neurons significantly increased fluorescence recovery and, therefore, translation of dendra2$_{actin}$ (Fig. 3A). In contrast, treatment of $Slack^{-/-}$ neurons with niclosamide did not stimulate fluorescence recovery but produced a small decrease in recovery. The difference between the small off-target effects of niclosamide in HEK cells and cortical neurons may reflect differences in the regulation of β-actin translation in these cell types. We also observed a higher number of outliers in FRAP recovery in DMSO-treated Slack-WT neurons, which may be due to several factors. Unlike in HEK cells, translation regulation in neuronal cultures is more dynamic and influenced by the cellular environment, and primary neurons have lower and more variable transfection efficiency than HEK cells, leading to differences in reporter expression levels. It is also possible that, in the absence of an activator, Slack-WT neurons exhibit a broader range of translation activity, contributing to increased variability.

To determine whether the constitutive stimulation of dendra2$_{actin}$ translation by the *Slack-R455H* mutant that was detected in HEK cells also occurs in native neurons, we compared translation in wild-type neurons to that in neurons isolated from the heterozygous *Slack-R455H* mice described earlier. FRAP experiments were carried out on primary cortical neurons from both genotypes of mice transiently transfected with dendra2$_{actin}$. As in HEK cells, the *Slack-R455H* mutation caused a significant increase in fluorescence recovery of dendra2$_{actin}$ compared to that in wild-type neurons (Fig. 3B), demonstrating that the *Slack-R455H* phenotype of dysregulated translation occurs in cortical neurons.

The constitutive stimulation of the dendra2$_{actin}$ reporter translation by the *Slack-R455H* mutation in neurons implies that the translation of endogenous β-actin should also be comparably increased. To test this directly, we carried out puromycin labeling combined with a proximity ligation assay (PLA) using antibodies against puromycin and β-actin (Fig. 3, C and D). This assay specifically identifies local β-actin synthesis by staining individual puncta of newly translated protein (*45*, *46*). The number of puncta in a given region of a cell represents the number of β-actin transcripts that are being actively translated and serves as a measure of endogenous translation rate. These experiments were carried out using cortical neurons from wild-type and *Slack-R455H* mice. We examined translation levels in both the soma and neurites (within 100 μm of the soma) of cultured neurons independently because activity-dependent translation in neurons is often a highly localized process (*47*–*51*). While we found no difference in the number of PLA puncta in the soma of neurons from wild-type and *Slack-R455H* mice, neurons from

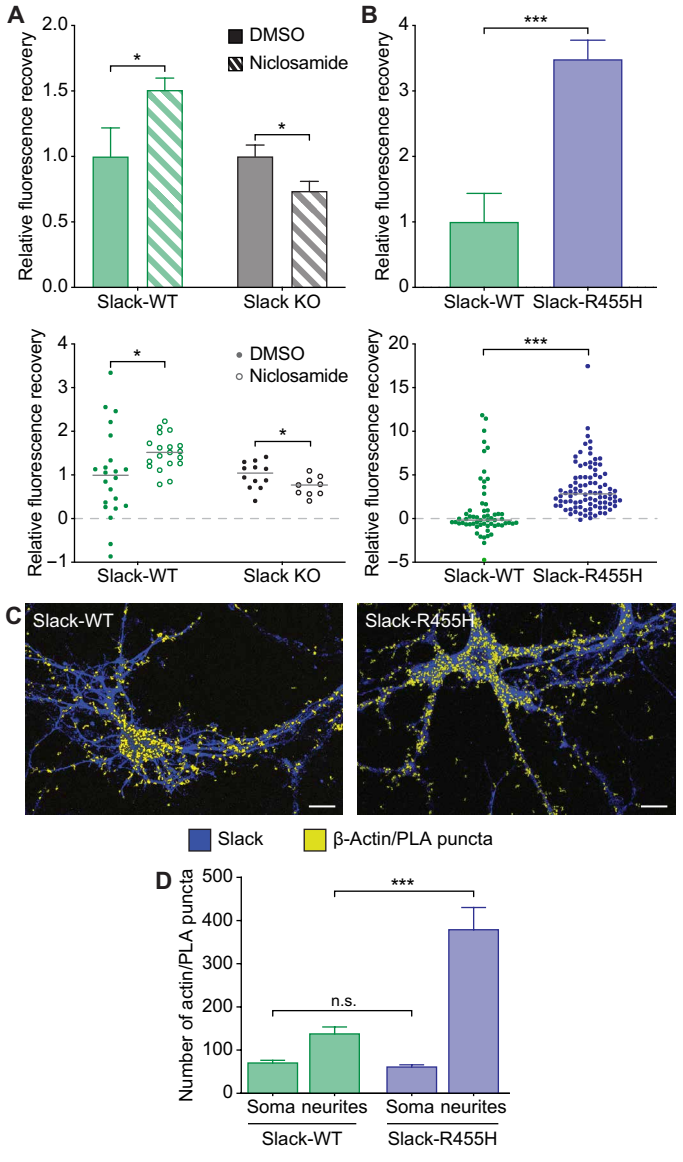

Fig. 3. Endogenous neuronal Slack channels regulate β-actin translation. (**A** and **B**) Bar graph of FRAP experiment in primary cortical neurons (A) from *Slack-WT* mice or $Slack^{-/-}$ mice with or without niclosamide (10 μM) ($n = 9$ to 22 cells) and (B) from *Slack-WT* or *Slack-R455H* mice ($n = 61$ to 91 cells). (**C**) Representative PLA images of individual neurons from *Slack-WT* (left) or *Slack-R455H* (right) mice. (blue, Slack; yellow, β-actin/PLA puncta; scale bars, 10 μm). (**D**) Quantification of puncta number from PLA images in the soma or neurites ($n = 17$ to 33 cells). All comparisons used unpaired *t* test. Data are expressed as means ± SEM. $^{*}P < 0.05$; $^{***}P < 0.001$. See data S2 for exact *P* values.

Slack-R455H mice had two to threefold more puncta within neurites, indicating higher levels of β-actin translation (Fig. 3, C and D). Our findings align with recent studies showing that K_{Na} channels are highly abundant in dendrites of cortical and hippocampal neurons (*52*). Overall, these results demonstrate that endogenous Slack activity regulates the translation of both the dendra2$_{actin}$ reporter and endogenous β-actin.

Slack-R455H mutation regulates translation initiation

We next characterized which step of RNA translation is regulated by the Slack channel. RNA translation is a cyclical process that includes initiation, elongation, and termination, each of which makes different predictions regarding the amount of nascent protein product associated with ribosomes (Fig. 4, A and B). If the *Slack-R455H* mutation were to increase translation by relieving stalling during elongation or termination, then the levels of nascent dendra2$_{actin}$ on ribosomes would decrease relative to those in cells expressing wild-type Slack or not expressing the channel (Fig. 4A). In contrast, increased levels of nascent dendra2$_{actin}$ associated with ribosomes would predict increased initiation of translation (Fig. 4B).

To differentiate between these two possibilities, we isolated ribosomes to measure the amount of bound dendra2$_{actin}$. Ribosomes were pelleted by centrifugation on a sucrose cushion according to a previously established protocol (*53*). A validation experiment revealed that cytoplasmic proteins were found exclusively in the supernatant, while ribosomal proteins were found only in the pellet (fig. S2, A and B). Membrane proteins, however, also pelleted with the ribosomal fraction. While most dendra2 was in the cytosolic fraction, a small portion was found in the pelleted fraction, presumably ribosome-bound dendra2. However, because our original dendra2$_{actin}$ construct

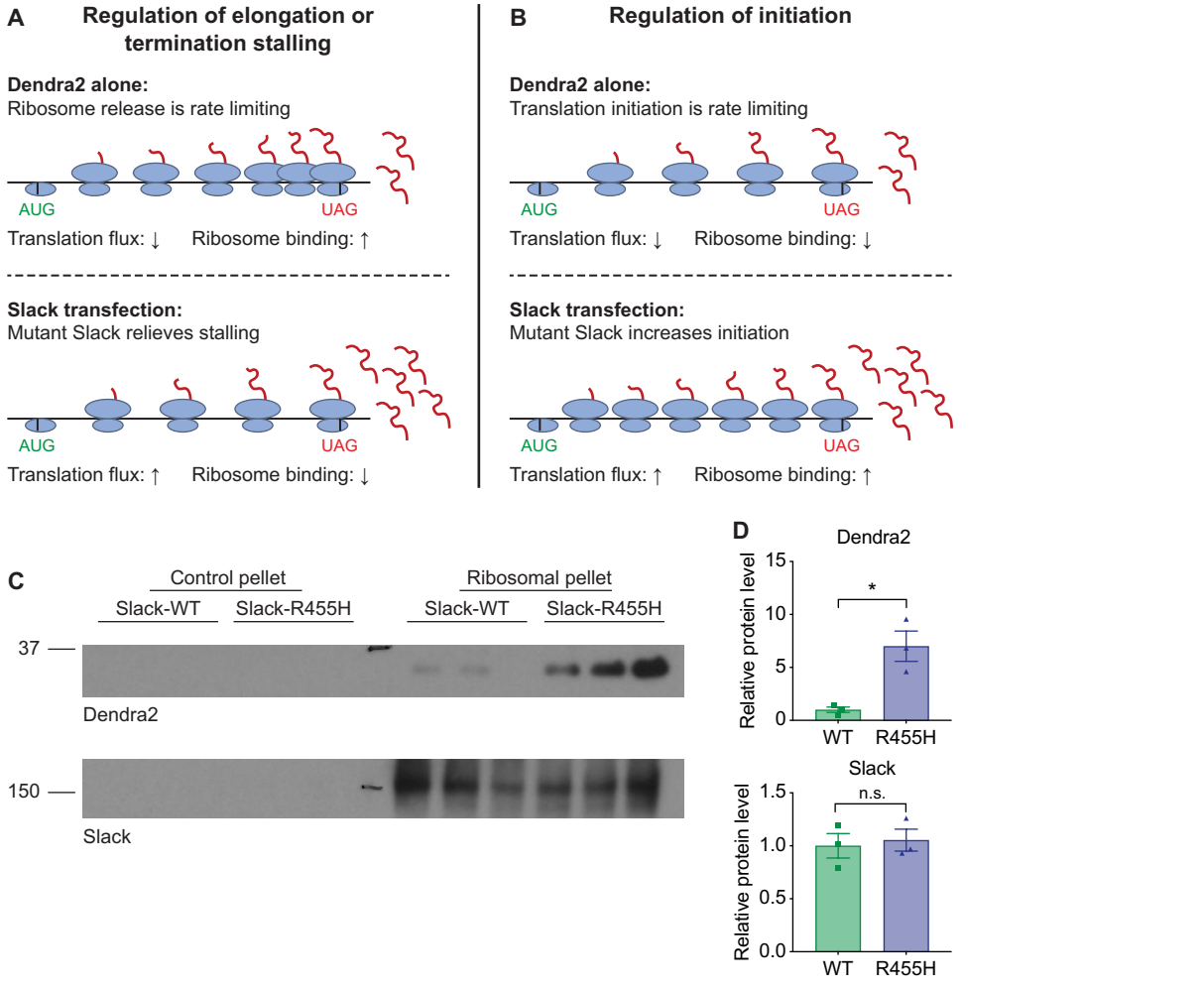

Fig. 4. *Slack-R455H* regulates translation initiation. (**A**) Model where Slack regulates translation through elongation or termination stalling. Top: In cells without Slack, ribosomes stall on dendra2 mRNA during elongation or termination. This leads to low total translation levels but high ribosome binding. This requires a secondary mechanism that stalls ribosomes under baseline conditions, such as stalling through UPF3B or FMRP. Bottom: When mutant Slack is present, ribosome stalling is relieved, leading to increased total translation levels but decreased ribosome binding. (**B**) Model where Slack regulates translation initiation. Top: In cells without Slack, translation occurs normally but with low total translation levels and ribosome binding. This model does not require a secondary mechanism to explain the baseline condition. Bottom: Mutant Slack increases the rate of translation initiation. This leads to both increased ribosome binding and total translation levels. (**C** and **D**) Ribosome binding of Δmyr-dendra2 in HEK cells 24 hours after co-transfection of Δmyr-dendra2 and *Slack-WT* or *Slack-R455H*. Slack staining represents total Slack in cell membrane and serves as loading control. Dendra2 levels are normalized by Slack level and then to WT level. Slack levels are normalized to WT level ($n = 3$, unpaired t test). Data are expressed as means ± SEM. *$P < 0.05$. See data S2 for exact P values.

contained a nonfunctional myristylation tag that normally targets protein to the membrane, we generated a construct without the myristylation tag (dendra2-Δmyr) to ensure that no fraction of dendra2$_{actin}$ was targeted to membrane. When we isolated ribosomes from cells co-expressing dendra2-Δmyr and Slack, we found that there was significantly more dendra2 bound to ribosomes in the presence of *Slack-R455H* than wild-type Slack (Fig. 4, C and D). As in previous experiments, Slack levels did not change. These results support the model proposed in Fig. 4B, suggesting that Slack regulates the initiation of translation. However, it remains possible that additional mechanisms, such as elongation and termination as shown in Fig. 4A, may also contribute to Slack-mediated translation regulation. Further investigation using elongation and initiation inhibitors will be necessary to clarify these potential mechanisms.

Slack channel activation triggers the redistribution of the FMRP/CYFIP1 complex

We further characterized the molecular mechanism by which Slack activity regulates translation initiation. In most mammalian mRNAs, translation initiation is mediated by a 5′ cap structure that binds eIF4E. A canonical mechanism through which the FMRP/CYFIP1 complex regulates mRNA translation is by inhibiting initiation through the sequestration of eIF4E (*25*, *27*). Dissociation of the FMRP/CYFIP1 complex from eIF4E is expected to release FMRP target mRNAs for translation (*25*). Because FMRP and CYFIP1 can be co-immunoprecipitated with Slack channels (*11*, *24*), we tested their role in Slack activity–dependent translation. We first determined whether the interactions of Slack channels with FMRP and CYFIP1 are altered by the disease-causing Slack mutation, *Slack-R455H*.

Immunoprecipitation (IP) from extracts of cerebral cortex of 2-month-old wild-type and *Slack-R455H* mice was carried out using an antibody against the N-terminal domain of Slack (*5*, *24*). We found that the levels of FMRP and CYFIP1 bound to Slack were higher in lysates from *Slack-R455H* mice than those from wild-type mice, with no difference in the levels of total or immunoprecipitated Slack in the two conditions (Fig. 5, A and C). Higher levels of phosphorylated FMRP [p-FMRP, a post-translation modification that regulates its activity; (*54*, *55*)] were also associated with the *Slack-R455H* mutant channel. To determine whether the increased binding of FMRP/CYFIP1 to Slack alters the amounts of FMRP/CYFIP1 bound to the translation initiation factor eIF4E, IP was carried out using an anti-eIF4E antibody. We found decreased levels of FMRP, p-FMRP, and CYFIP1 immunoprecipitated by an eIF4E antibody in lysates from *Slack-R455H* mice (Fig. 5, B and C). There were no differences in levels of eIF4E between the two conditions.

We next tested whether the dissociation of FMRP/CYFIP1 from eIF4E occurs in response to pharmacological activation of the channel expressed in a mammalian cell line. Co-IP experiments were carried out using HEK cells expressing wild-type rat Slack or the *Slack-R455H* mutant channel, treated with or without the Slack channel activator niclosamide (*24*, *41*, *56*). Transfection with Slack constructs did not alter the levels of FMRP, p-FMRP, and CYFIP1 in cell lysates (Fig. 6, A and D). Both in cells expressing the wild-type and *Slack-R455H* mutant channels, however, treatment with niclosamide resulted in higher levels of FMRP, p-FMRP, and CYFIP1 bound to Slack (Fig. 6, B and D) but lower levels bound to eIF4E (Fig. 6, C and D). Collectively, our results indicate that activation of Slack channels triggers the redistribution of the FMRP/CYFIP1 complex, with decreased binding of the complex to eIF4E and increased binding to Slack channels.

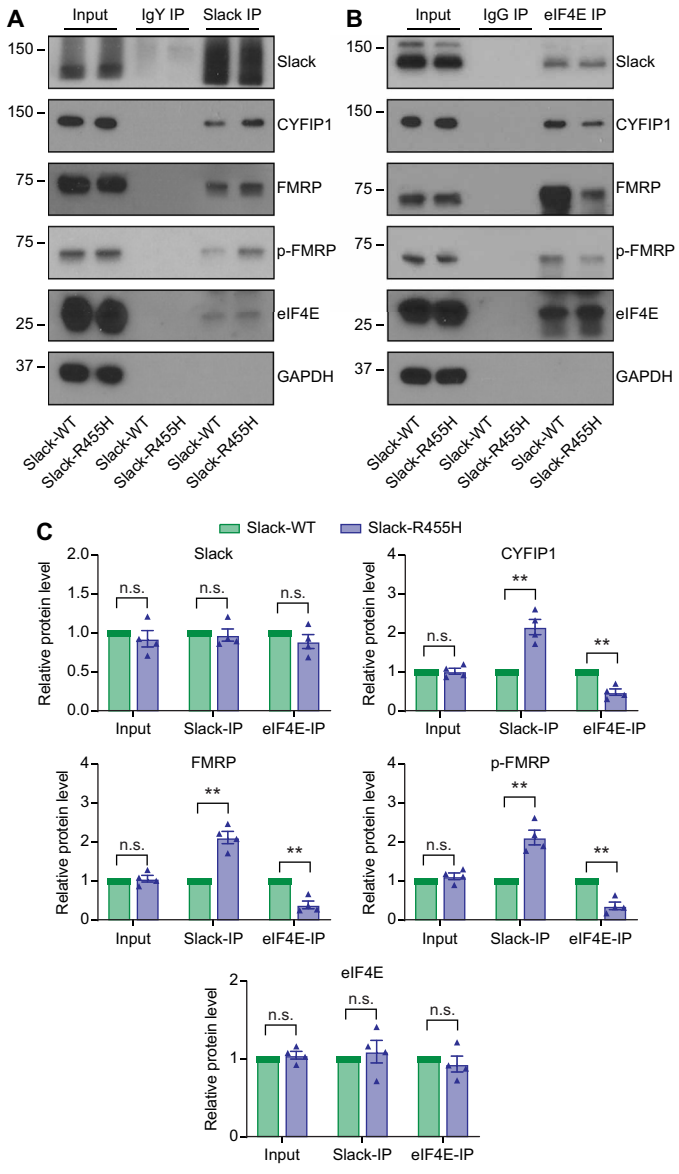

Fig. 5. *Slack-R455H* mutation triggers the redistribution of the FMRP/CYFIP1 complex. (**A** and **B**) IP of Slack (A) or eIF4E (B) from mouse cerebral cortex. (**C**) Quantification of Western blots in (A) and (B). Input, Slack IP, and eIF4E IP samples are normalized by GAPDH, Slack, and eIF4E levels, respectively, followed by normalization to Slack-WT level ($n = 4$ mice, paired t test). Data are expressed as means ± SEM. $^{**}P < 0.01$. See data S2 for exact P values.

FMRP and CYFIP1 are required for Slack activity–dependent translation

The recruitment of FMRP and CYFIP1 to the Slack channel complex, resulting in reduced levels of both proteins bound to eIF4E, provides a ready explanation for increases in translation upon channel activation. If this is the case, then deletion of FMRP and CYFIP1 would unlink Slack from the translation machinery. To test this hypothesis, we suppressed FMRP and CYFIP1 expression in HEK cells using small interfering RNA (siRNA). Western blots revealed that the siRNAs are highly effective in reducing total levels of FMRP and CYFIP1 but do not affect levels of Slack protein (Fig. 7, A to D).

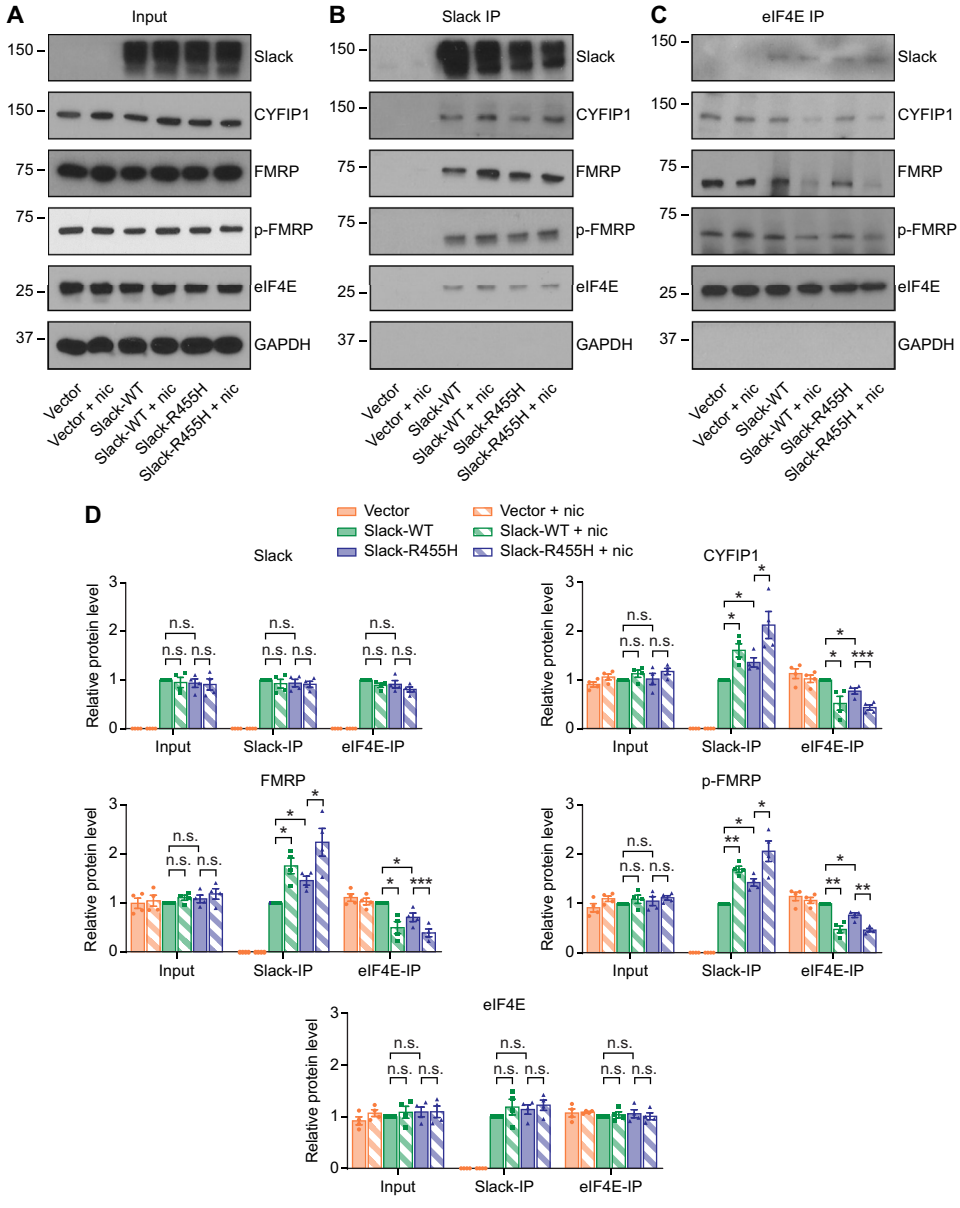

Fig. 6. Slack channel activation triggers the redistribution of the FMRP/CYFIP1 complex. (**A**) Western blotting showing protein expression in HEK cells transfected with vector control, rat wild-type Slack (*Slack-WT*), or *Slack-R455H* treated with or without niclosamide (nic; 5 μM, 30 min). (**B** and **C**) IP of Slack (B) or eIF4E (C) in HEK cells treated with/without niclosamide (5 μM, 30 min). (**D**) Quantification of Western blots in (A) to (C). Input, Slack IP, and eIF4E IP samples are normalized by GAPDH, Slack, and eIF4E levels, respectively, followed by normalization to Slack-WT level ($n = 4$ replicates, paired t test). Data are expressed as means ± SEM. $^{*}P < 0.05$; $^{**}P < 0.01$; $^{***}P < 0.001$. See data S2 for exact P values.

We co-transfected dendra2 with either *fmr1* or *cyfip1* siRNA or with both siRNAs together into hSlack-expressing HEK cells. After 48 hours, cells were incubated with the Slack activator niclosamide or with DMSO alone for 90 min before protein extraction. Treatment with either *fmr1* or *cyfip1* siRNA alone did not prevent an increase in levels of dendra2 in response to the channel activator (Fig. 7, E to H). Combined treatment with both siRNAs, however, eliminated the effect of niclosamide, while treatment with the negative control siRNAs had no effect on the ability of the activator to simulate dendra2 synthesis (Fig. 7, I and J). Neither the siRNA for *fmr1* and *cyfip1* nor the negative control had any effect on levels of Slack. Last, we also carried out FRAP experiments in hSlack-expressing HEK cells treated with *fmr1* and *cyfip1* siRNAs or the negative control, with and without niclosamide. Again, reducing both translation regulators fully eliminated the ability of niclosamide to stimulate the synthesis of the dendra2$_{actin}$ reporter in the FRAP assay (Fig. 7K), confirming a requirement for FMRP and CYFIP1 for Slack activity–dependent translation.

DISCUSSION

We have found that activation of Slack Na^+-activated K^+ channels increases the rate of translation initiation of a dendra2$_{actin}$ reporter mRNA in mammalian cell lines and enhances the synthesis of native β-actin itself in cortical neurons. This effect can be recapitulated in

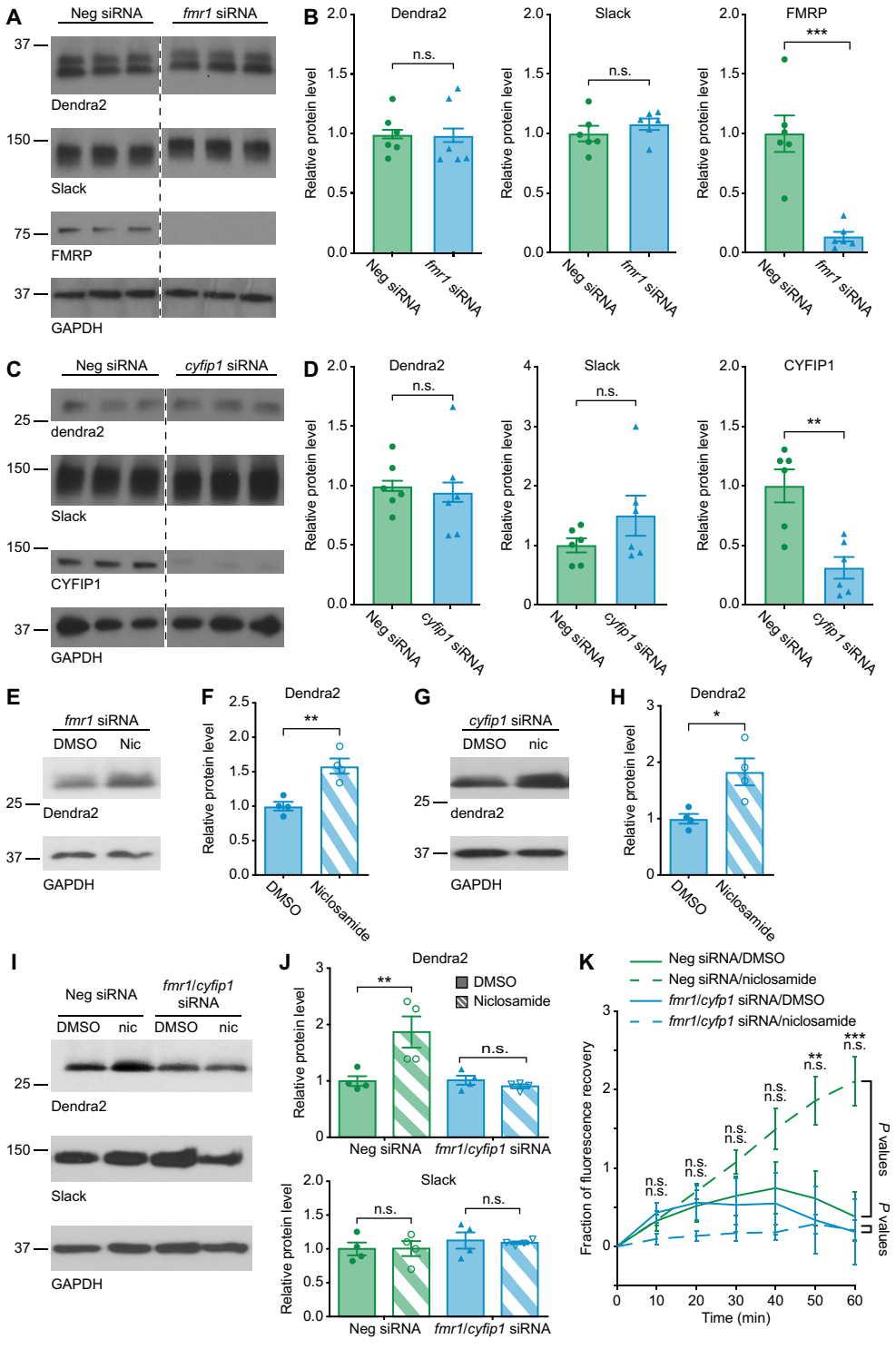

Fig. 7. FMRP and CYFIP1 are required for Slack activity–dependent translation. (**A** to **D**) Effect of knockdown of FMRP [(A) and (B)] or CYFIP1 [(C) and (D)] on dendra2$_{actin}$ expression in HEK cells. Cell extraction was carried out 24 hours after triple transfection of dendra2$_{actin}$, rat *Slack-WT*, and *fmr1* siRNA cocktail or *cyfip1* siRNA or negative (Neg) siRNA control. Protein levels were normalized to GAPDH level, followed by normalization to neg siRNA level ($n = 6$ replicates, unpaired *t* test). (**E** to **J**) Effect of knockdown of FMRP [(E) and (F)] or CYFIP1 [(G) and (H)] or both [(I) and (J)] on niclosamide-induced translation of dendra2$_{actin}$ in hSlack-expressing HEK cells. Cell extraction was carried out 48 hours after co-transfection of dendra2$_{actin}$ with *fmr1* siRNA cocktail, *cyfip1* siRNA, or both *fmr1* and *cyfip*1 (*fmr1/cyfip1*) siRNAs or negative siRNA control, with or without Slack activator niclosamide (nic; 10 μM, 90 min) treatment. $n = 4$ replicates for all experiments. [(F), (H), and (J)] Paired *t* tests. (**K**) Time course of FRAP experiment in hSlack-expressing HEK cells 48 hours after co-transfection of dendra2$_{actin}$ with *fmr1/cyfip1* siRNAs or negative siRNA control, with or without niclosamide (10 μM, 60 min). *P* values represent differences between indicated groups ($n = 9$ to 21 cells, two-way repeated-measures ANOVA with post hoc comparisons with Holm-Šídák correction). Data are expressed as means ± SEM. $^*P < 0.05$; $^{**}P < 0.01$; $^{***}P < 0.001$. See data S2 for exact *P* values.

cell lines expressing either rat or human Slack channels and is blocked by reducing expression of both FMRP and CYFIP1. Mechanistically, we observe that this Slack activity–dependent translation is coupled to the redistribution of the FMRP/CYFIP1 complex. Channel activation increases the binding of these two regulatory proteins to the channel and decreases their binding to the translation initiation factor eIF4E (*25*). The gain-of-function *Slack-R455H* mutation similarly enhances the binding of FMRP/CYFIP1 to the channel, leading to less binding to eIF4E, which results in constitutive activation of translation in both neurons and cell lines (Fig. 8). Mice that are heterozygous for *Slack-R455H* have spontaneous seizures and persistent interictal spikes and the corresponding mutation in humans causes early onset epilepsy with severe intellectual disability (*10*, *35*).

Slack channel activity is regulated by the binding of FMRP (*11*, *12*). In neurons, intracellular injection of the peptide FMRP(1-298) rapidly increases the native Slack current and produces narrowing of action potentials (*12*). In addition, single-channel open probability is increased when FMRP(1-298) is added directly to the cytoplasmic face of Slack channels in excised patches, further supporting a direct regulation of Slack by FMRP (*11*). The translational regulation of Slack through FMRP raises the possibility of a cyclical positive feedback loop between FMRP binding and Slack channel activation, which could theoretically lead to uncontrolled translation. However, Slack channel activation is primarily dependent on Na^+ influx through various pathways (*1*–*3*). While FMRP binding can enhance Slack channel activity, the overall level of sodium influx remains the key determinant of Slack activation. As a result, upstream Na^+ dynamics may provide a natural limit to Slack activation and prevent uncontrolled neuronal excitability and excessive translation. As Slack is a potassium channel, its activation will also hyperpolarize the cell, thereby shutting down Na^+ entry and further Slack activation, preventing runaway translation. In addition, while our current findings demonstrate that Slack channel activation directly regulates translation, future studies should explore whether changes in neuronal activity, such as those induced by electrical or chemical stimulation, affect channel-FMRP interactions and translational regulation. Furthermore, these findings raise the question of whether the interactions of FMRP with other ion channels (*13*–*19*) influence protein synthesis or other biological processes regulated by FMRP. For example, although we did not find an increase in translation of dendra2$_{actin}$ reporter with pharmacological stimulation of BK channels, FMRP binding to the channels may alter its availability for other functions, such as mRNA transport or other aspects of cellular metabolism (*57*–*59*).

Loss of expression of FMRP in humans results in fragile X syndrome (FXS), the leading inherited cause of intellectual disability and autistic spectrum behavior, with co-occurring seizures, anxiety, hyperactivity, hypersensitivity, and hyperarousal (*20*, *60*). Although FMRP has been extensively studied for its role in binding neuronal mRNAs to regulate their translation, it remains unclear whether its primary function is to activate or repress translation, affect RNA stability or trafficking, or control other aspects of RNA metabolism (*26*, *30*, *59*, *61*–*63*). Notably, FMRP binds to up to 4% of total brain mRNAs (*64*, *65*) and previous work has shown that the Slack-FMRP complex contains known mRNA targets of FMRP, such as *Map1b* and *Arc* (*11*). While our study found that activation of Slack channels specifically affects the translation of actin without influencing global translation, it remains to be determined whether the translation or trafficking of other targets of FMRP are also regulated by Slack channel activity.

One well-established mechanism of translational control involves FMRP forming a complex with CYFIP1 (*25*). This complex inhibits translation by binding to the initiation factor eIF4E, which prevents eIF4E from binding to eIF4G, a critical step for translational initiation. The FMRP-CYFIP1-eIF4E complex is present in dendritic spines and actively participates in the local regulation of protein synthesis, including actin, during synaptic activity (*27*). Synaptic activation by BDNF or mGluR promotes the release of FMRP and CYFIP1 from eIF4E and promotes local translation (*25*, *66*). Additionally, pharmacological inhibition of the eIF4E-eIF4G interaction with 4EGI-1 unlinks CYFIP1 from the protein synthesis machinery in FXS mice (*27*). In the present study, we found that activation of Slack channels

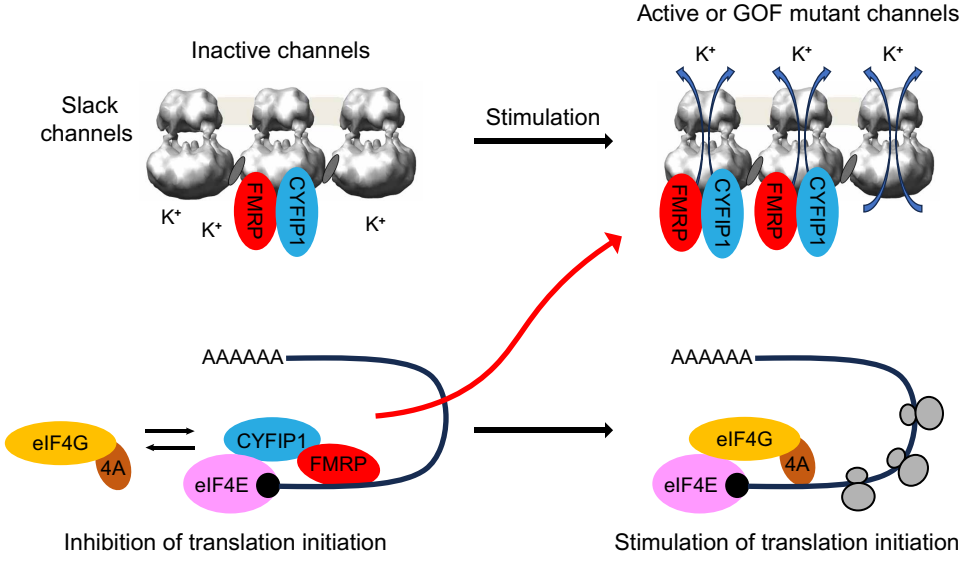

Fig. 8. Model of potential mechanism of Slack activity–dependent translation. When Slack channels are inactive, the FMRP/CYFIP1 complex binds to eIF4E in a translation initiation suppression complex. When Slack channels are activated or when gain-of-function (GOF) channels are present, the FMRP/CYFIP1 complex moves from the eIF4E complex to Slack channels, allowing translation to resume.

increases the binding of both FMRP and CYFIP1 to the channel while reducing their binding to eIF4E. This suggests that the FMRP/CYFIP1 complex shuttles between eIF4E and the Slack channel, connecting translation regulation to channel activity, both of which are dysregulated in Slack mutant mice (Fig. 8). However, the FMRP/CYFIP1 complex may also originate from translationally stalled FMRP granules, where FMRP regulates mRNA transport and localized translation (*22*, *23*). Given the broad distribution of FMRP across different cellular regions, it is plausible that Slack activation influences FMRP redistribution beyond eIF4E-associated complexes. Additional experiments, including PLAs and ribosome profiling, will be necessary to gain further insight into this mechanism. We also found that suppression of both FMRP and CYFIP1 fully unlinked Slack channel activity from changes in translation. Perhaps unexpectedly, removal of these translation regulators did not increase basal levels of translation of the dendra2$_{actin}$ reporter construct. One possible explanation is that FMRP and CYFIP1 independently regulate the expression of numerous cellular proteins, including other regulators of translation, in both positive and negative directions to maintain translational homeostasis. Further studies will be required to identify the subset of mRNAs that bind the Slack-FMRP-CYFIP1 complex and determine whether Slack channel activation selectively influences FMRP target mRNAs.

Regulation of the translation of the dendra2$_{actin}$ reporter by Slack requires the UTR regions of the β-actin gene. β-actin translation was selected as potential target of Slack regulation for several reasons. First, β-actin mRNA is a known binding target of FMRP (*30*). As previous experiments demonstrated a functional interaction between Slack and FMRP, targets of FMRP binding are an obvious initial set of targets to examine (*12*). β-Actin is also known to be expressed both pre- and postsynaptically, where its translation is upregulated following synaptic stimulation (*31*, *48*), as would be expected of targets of Slack activity–dependent translation (*1*, *5*). Although we found that global translation levels are not affected by the *Slack-R455H* mutation in heterologous cells, it is probable that other subsets of neuronal mRNA are also sensitive to Slack channel activation. For example, levels of the sodium channel $Na_V1.6$ are substantially increased in the cerebral cortex of mice with the *Slack-R455H* mutation (*67*). Further study will be required to determine whether Slack channel activation alters the translation of $Na_V1.6$ and other mRNAs across various neuronal cell types.

Our findings strongly suggest that severe intellectual disability, a hallmark of Slack-related epilepsies, does not result from the effects of the mutations on neuronal excitability alone. One of the conditions produced by gain-of-function mutations is autosomal dominant sleep-related hyperkinetic epilepsy (ADSHE). Patients with ADSHE caused by Slack mutations have a very high chance of developmental delay and intellectual disability (*8*, *68*–*70*). ADSHE is, however, also caused by mutations in the nicotinic acetylcholine receptors CHRNA2, CHRNA4, or CHRNB2 (*69*). These patients almost always have normal cognitive development, despite identical seizure presentation to that caused by Slack mutations (*69*, *70*). Our data suggest that, under normal physiological conditions, activation of Slack channels stimulates the translation of mRNAs as part of the normal homeostatic process. Under pathological conditions, this translation regulation becomes constitutively active. This strongly suggests that the disruption of Slack activity–dependent protein synthesis, rather than the seizures themselves, is a major factor that accounts for the severity of the effects of Slack mutations in humans. This conclusion is also consistent with the fact that dysregulation of translation is a recognized cause of intellectual disability (*59*, *68*, *71*–*74*).

MATERIALS AND METHODS

Experimental design

The first objective of this study was to determine whether a gain-of-function Slack channel mutation regulated the translation of a β-actin reporter construct in HEK cells. This was accomplished using transient transfection and Western blotting. The next objective was to determine whether channel activity is sufficient to stimulate translation. This was accomplished by tracking FRAP of the reporter construct. The next objective was to determine whether Slack activity–dependent translation is present in cortical neurons and whether endogenous β-actin is regulated by this mechanism. This was accomplished using neuron cell culture, FRAP, and a PLA. The final objective was to identify the mechanism of Slack activity–dependent translation. This was accomplished using ribosome isolation, co-IP, and Western blotting.

Drugs

All pharmacological agents were obtained as dry compounds and dissolved in DMSO (AmericanBio) to form 1000× stock solutions. Niclosamide (Santa Cruz Biotechnology) was diluted to a final concentration of 5 or 10 μM as noted, quinidine (Tocris Bioscience) was diluted to a final concentration of 500 μM, and NS1619 (MedChemExpress) was diluted to a final concentration of 30 μM.

DNA constructs and subcloning

Rat-Slack-B-mCherry (*Slack-WT*), *Slack-R455H*, and mCherry-alone (empty vector) were engineered and characterized as described (*7*, *75*). The pCS2-myrDendra2-Actb5′UTR3′ (dendra2$_{actin}$) construct was a gift from D. Benson (Icahn School of Medicine). myrDendra2-Actb5′UTR3′ subcloning into pEGFP-C1 vector (dendra2-C1) was performed with restriction enzyme cloning using NEBNext Ultra II Q5 Master Mix (New England BioLabs) using the following primers: forward primer: ATA**ACTAGT**ATGGGCACGGTGCTGTC; reverse primer: AAT**GGTACC**TAGAAGCATTTGCGTCGAGTCTT); bold represents restriction enzyme target sequences. Subcloning PCR product and pEGFP-C1 backbone were cut using KpnI–HF and SpeI–HF restriction enzymes (New England BioLabs) and ligated using Quick Ligase Kit (New England BioLabs) according to the manufacturer's protocols. The myristylation tag of dendra2 was removed to generate pCS2-ΔmyrDendra2-Actb5′UTR3′ (Δmyr-dendra2) using the Q5 Site-Directed Mutagenesis Kit, substituting NEBNext Ultra II Q5 Master Mix for the kit's polymerase (forward primer: AACACCCCGGGAATTAACC; reverse primer: CATGGCGAACTGGTGGCG). All constructs were verified by DNA sequencing from Yale Keck facility.

Cell culture and transfection

HEK 293 T cells [American Type Culture Collection (ATCC)] were maintained in high-glucose Dulbecco's modified Eagle's medium (DMEM) (Gibco). Medium was supplemented with 10% fetal bovine serum (FBS; MilliporeSigma) and 1% penicillin-streptomycin solution (MilliporeSigma) incubated at 37°C with 5% CO_2. HEK cells stably transfected with human Slack (*hSlack-WT*) were obtained as a gift from Autifony Therapeutics. *hSlack-WT* cells were cultured in medium supplemented with G418 (500 μg/ml; Thermo Fisher Scientific). Cells were split every 3 to 4 days when confluent using TrypLE

Express (Gibco). For all immunoblotting and imaging experiments, cell dishes were precoated with 0.002% poly-L-lysine (MilliporeSigma) for 15 min followed by 2× wash with water. Cells were plated on dish in 2 ml of DMEM at a density such that they were confluent 48 hours after plating. For standard immunoblotting, IP, and imaging experiments, cells were plated in 35-mm dishes (HEK, 2.5E5 cells; *hSlack-WT*, 4E5 to 4.5E5 cells). For ribosome binding assay experiments, cells were plated in 60-mm dishes (2.5× all 35-mm values; all further quantities listed are for 35-mm dishes unless specified). Transient transfection was performed 24 hours after plating using Lipofectamine 2000 (Thermo Fisher Scientific) according to the manufacturer's protocol. Cells were transfected with 500 ng of dendra2 construct and/or 500 ng of Slack construct, as specified, in 500 µl of optiMEM (Gibco) medium with 5 µl of lipofectamine.

CHO cells (ATCC) were maintained similar to HEK cells with the following differences: Culture medium was Iscove's modified Eagle's medium (Invitrogen) supplemented with 10% FBS, 1% penicillin-streptomycin solution, and 1% hypoxanthine-thymidine supplement (Invitrogen). Cells were split approximately every 2 days. CHO cells were plated at 2.5E5 cells per dish in 35-mm dishes.

Animals/primary neuronal culture

Rodents were handled in accordance with protocols approved by the Yale University Institutional Animal Care Committee (approval number and license number are 2025-07842). Mice were housed on a 12-hour/12-hour light/dark cycle with access to food and water ad libitum. Slack WT mice (*Slack-WT*) were C57BL/6J mice. Slack KO (*Slack*$^{-/-}$) and *Slack-R455H* mice were generated as previously described (*35*, *76*). Genotyping was performed by ear clip biopsy-derived genomic DNA using established PCR protocols.

For IP experiments, cortex lysates from 2-month-old mice were used. Primary cortical neurons were prepared from postnatal day 2 (P2) to P3 mice (for niclosamide experiments) or from embryonic day 16 (E16) to E17 mouse embryos (for knock-in mouse experiments) as described previously with modifications specific for this study (*77*). After isolation of cortex from neonatal or embryonic brains, neurons were dissociated and seeded (on coverslips inside a six-well plate: 2E5 cells per six-well plate) onto plates containing neurobasal medium supplemented with B27 (Gibco), 5% FBS (Gibco), L-glutamine, and antibiotics (Gibco). After 2 hours of incubation, primary cultures were maintained in neurobasal medium without FBS in a 5% CO_2 and 20% O_2 incubator at 37°C. Subsequently, half the medium was replaced every 2 days. Neuronal cultures were transfected using Lipofectamine 2000 and experiments were performed at day in vitro 14 (DIV14) to DIV21. Depending on the culture density, 0.1 to 0.5 µg of dendra2 DNA vector was used for transfection.

Puromycin assay

For standard immunoblotting or IP experiments, puromycin incorporation protocols were identical. Before protein extraction, cells were incubated with puromycin (10 µg/ml), dihydrochloride (MilliporeSigma) for 10 min at 37°C. Cells were immediately placed on ice and protein extraction was begun.

RNA interference

FMRP knockdown was performed using a silencing RNA (siRNA) cocktail made with equal parts of three Silencer Select siRNA against the *fmr1* gene (Thermo Fisher Scientific, s5315, s5316, and s5317) (*24*). CYFIP1 knockdown was performed using Silencer Select siRNA against the *cyfip1* gene (Thermo Fisher Scientific, s23242) (*24*). Silencer Select Negative Control 1 (Thermo Fisher Scientific) was used as a control. For transfection, 50 pmol of siRNA of either cocktail or both together was co-transfected with DNA plasmids using Lipofectamine 2000 as described above. The negative controls used the same amount of total siRNA.

Immunoblotting/co-IP

Protein lysates from HEK cells or 2-month-old mice frontal cortex were prepared using Pierce IP Lysis Buffer (Thermo Fisher Scientific) supplemented with cOmplete EDTA-free Protease Inhibitor Cocktail (MilliporeSigma) according to the manufacturer's protocol. Protein quantification was performed using Pierce BCA Protein Assay Kit (Thermo Fisher Scientific). For standard immunoblotting experiments or co-IP input controls, 7.5 µg of protein was loaded onto precast 15-well 4 to 15% Mini-Protean TGX Stain Free Gels (Bio-Rad).

For co-IP experiments, 187.5 µg of protein was transferred to 1.5-ml Eppendorf tubes. Sample was precleared with 70 µl of Pierce A/G agarose beads (Thermo Fisher Scientific) or Anti–immunoglobulin Y (IgY) PrecipHen beads (AvesLabs) (50% v/v Pierce IP lysis buffer). Tubes were incubated at 4°C for 1 hour on rotator. Samples were centrifuged at 3000 rpm at 4°C for 2 min. Sample (75 µg) was incubated at 4°C overnight on rotator with 5 µg of mouse anti-puromycin antibody (MilliporeSigma, MABE343), rabbit anti-eIF4E (Abcam, ab33766), chicken anti-Slack antibody, or IgG (Santa Cruz Biotechnology, sc-2025) or IgY (AvesLabs) control antibodies. Beads (30 µl) were added to samples, which were then incubated at 4°C for 2 hours on rotator. Samples were centrifuged at 3000 rpm at 4°C for 1 min to collect beads, which were washed seven times with Pierce IP Lysis Buffer. Protein was eluted by incubation with 50 µl of 2× Laemelli Buffer (Bio-Rad) at room temperature for 30 min on rotator. Mini-protean gel was loaded with 15 µl of eluted sample.

For all immunoblotting experiments, gels were processed and blots were developed as previously described (*12*). Primary and secondary antibodies were used at the following concentrations: anti-dendra2, 1:5000 (OriGene: TA150090); anti-Slack, 1:5000 (Aves labs, custom); anti-puromycin, 1:1000 (MilliporeSigma, MABE343); anti-FMRP, 1:2000 (MilliporeSigma, MAB2160); anti–p-FMRP, 1:1000 (Thermo Fisher Scientific, PA5-35389); anti-CYFIP1, 1:500 (Santa Cruz Biotechnology, sc-49932); anti-eIF4E, 1:1000 (Abcam, ab33766); anti–glyceraldehyde-3-phosphate dehydrogenase (GAPDH), 1:1000 (Santa Cruz Biotechnology, sc-32233); anti-rabbit horseradish peroxidase (HRP), 1:1000 (Thermo Fisher Scientific, 32460); anti-mouse HRP, 1:1000 (Thermo Fisher Scientific, 32430); anti-goat, 1:10,000 (Thermo Fisher Scientific, 31402); and anti-chicken HRP, 1:20,000 (Jackson Laboratories, 703-035-155). Wash steps were performed with three 10-min washes. When multiple antibodies were stained successively on the same blot, blots were stripped as necessary with 5 ml of Restore Plus Western blot Stripping Buffer (Thermo Fisher Scientific) followed by three 5-min washes. Protein bands were analyzed with ImageJ [National Institutes of Health (NIH)] software. Where applicable, blots were normalized to GAPDH or Slack levels followed by normalization to the level of the denoted control group, as described in the figure legends. Both normalization steps were performed on a per-blot basis. When individual blots contained one sample of each condition (Figs. 5, 6, and 7, E to J), paired *t* tests were performed. When individual blots contained multiple samples of each condition (Figs. 1, 4, and 7, A to D), unpaired *t* tests were performed.

Imaging experiments

For HEK and CHO cell imaging experiments, cells were replated 12 (baseline fluorescence) or 36 (FRAP) hours after transfection. Cells were rinsed twice with phosphate-buffered saline (PBS) followed by a 5-s rinse with 0.5 ml of TrypLE Express. Cells were replated onto fresh 35-mm dishes coated with poly-L-lysine (as described above) at a density of 1.5E5 cells/dish in 2 ml of high-glucose DMEM. Cells were imaged 12 to 24 hours after replating. Medium was changed to 2 ml of phenol red–free DMEM (Gibco) supplemented with 25 mM Hepes and 4 mM L-glutamine with any denoted drugs 30 min (except where noted) before imaging.

HEK and CHO cell imaging experiments were performed with semiautomated imaging using a Scientifica Hyperscope multiphoton system using custom-built Matlab scripts. For baseline imaging experiments, the only active user input is initial focal plane selection. The program selects six arbitrary fields of view (FOVs). For FRAP experiments, the user manually selects FOV. One to two FOVs are imaged per plate, so manual selection is desired to ensure that FOV contains enough cells without any overbright cells or debris. Once FOV are selected, the program takes initial *Z*-stack image of FOV and automatically segments image to identify all cells from sum-intensity projection of *Z*-stack image. In FRAP experiments, program photobleaches identified cells by about 50% and takes a post-bleach *Z*-stack image. Bleaching is performed using a high-laser power and high-density imaging. These steps are performed successively for each FOV. After the initial imaging and bleaching, microscope returns to each FOV at set time intervals, taking a time course of recovery *Z*-stacks. For all automated imaging, fluorescence levels are automatically calculated for all cells and FOV. Range for *Z*-stack is determined by identifying focal plane edges past which total FOV fluorescence is below a threshold value. This automation allows substantial imaging throughput, prevents user-generated bias in both focal plane selection and cell detection, and maximizes reproducibility. Imaging parameters are as follows: acquisition system, GalvoImaging; laser wavelength, 960 nm; beam power, 20%; photomultiplier tube gain, 600; image resolution, 1024 pixels; frame/slice, 4; slice number, 5; focus threshold, 600 arbitrary units (a.u.); bleach power, 40%. Cells were filtered to include only healthy bleached cells. HEK cell inclusion criteria were as follows: minimum bleach, 20% baseline reduction; maximum bleach, 75% baseline reduction; minimum fluorescence (at $t = 0$), 25 a.u.; maximum fluorescence (at $t = 0$), 2000 a.u.; and minimum recovery (at $t = 60$), 0 a.u. Quinidine and siRNA FRAP experiment used the following modifications due to laser recalibration and software updates. Quinidine: beam power, 25%; bleach power, 85%; manual segmentation (for bleaching only). siRNA: beam power, 25%; no bleaching (does not alter observed recovery, as seen with negative control siRNA); maximum time point 1 decrease, 50% baseline reduction (removes cells with large fluctuations); and recovery time point extremes, 75%, 400% (removes outlier cells). Due to differences in CHO cell bleaching and fluorescence levels, CHO cell inclusion criteria were different as follows: minimum bleach, not used; minimum fluorescence (at $t = 0$), 20 a.u.; and minimum recovery (at $t = 30$), 0 a.u. Using the FRAP assay, we found that the translation inhibitor, anisomycin, prevents fluorescence recovery, demonstrating that fluorescence recovery is a valid measure of translation levels (DMSO, mean recovery after 60 min = 0.22 ± 0.037, $n = 3$; anisomycin, mean recovery after 60 min = 0.057 ± 0.031, $n = 4$; Student's *t* test, $P = 0.019$)

FRAP experiments in neurons were performed manually using a Zeiss Axiovert 200 epifluorescence microscope 24 hours post-transfection. Drug was directly added to medium before imaging. After taking baseline image, cells were bleached for 2 min at full laser power, after which post-bleach image was taken. Recovery period for neurons was 5 min. Fluorescence intensity (center of the soma) was analyzed using ImageJ software. No inclusion criteria were used for neuron FRAP as recovery was calculated for individual cells at a single time point and fit a normal distribution (Fig. 3, A and B, bottom).

Real-time qPCR

For qPCR experiments, mRNA was isolated using the RNeasy Mini Kit (QIAGEN), and cDNA was generated using the ProtoScript II Reverse Transcription Kit (New England BioLabs). qPCR was performed on a LightCycler 480 real-time PCR system (Roche) using PowerUp SYBR Green Master Mix (Thermo Fisher Scientific) according to the manufacturer's instructions. RNA levels for each condition were calculated using the single-delta cycle threshold (CT) method with *Gapdh* as the housekeeping gene. Data for dendra2 and Slack represent the mean mRNA level of two independent primer pairs for a given sample. See table S1 for primer sequences.

Ribosome binding assay

Ribosome binding assay is adapted from previously published ribosome profiling protocol (*53*). Above protein extraction protocol was used with the following changes: Cells were washed three times with 2 ml of ice cold PBS spiked with cycloheximide (CHX; 100 μg/ml) (Sigma-Aldrich). Lysis buffer was replaced with 500 μl of polysome lysis buffer: 20 mM tris (pH 7.4), 150 mM NaCl, 5 $MgCl_2$, 1 mM dithiothreitol (DTT), CHX (100 μg/ml), 1× Protease Inhibitor Cocktail, and 1% Triton X-100. Incubation at 4°C was not performed on rotator. Cells were triturated 10 times through a 26-gauge needle after 4°C incubation. Clarifying centrifugation was changed to a 10-min 5000*g* centrifugation followed by a 20,000*g* centrifugation. Last, samples were snap frozen in ethanol and dry ice and stored at −80°C until use.

For polysome isolation step, samples were diluted to 420 μg of protein in 240 μl of polysome lysis buffer. Ribonuclease (RNase) 1_f (2 μl; New England Biolabs) was added to samples and incubated at room temperature for 45 min under gentle agitation. Meanwhile, a 1 M (34% w/v) sucrose cushion was prepared: 20 mM tris (pH 7.4), 150 mM NaCl, 5 mM $MgCl_2$, 1 mM DTT, 1 mM sucrose, CHX (100 μg/ml), and SUPERase-In RNase Inhibitor (20 U/ml; Thermo Fisher Scientific). Sucrose cushion (2 ml) was added to 13 mm–by–51 mm Ultra Clear tubes (Beckman). After incubation, 200 μl of sample was gently added on top of sucrose cushion. Additional polysome lysis buffer was added to tubes to equalize mass (±5 mg). Ribosomes were pelleted by centrifugation in an SW 55 Ti rotor for 4.5 hours at 45,000 rpm. These conditions result in equal sedimentation to the conditions used by McGlincy and Ingolia (*53*)

After centrifugation, cushion fractions were saved as described in results. The pellet was extracted by adding 50 μl of 2× Laemelli Buffer and incubating for 10 min at 37°C. Tubes were briefly vortexed, and pellet fraction was transferred to a microcentrifuge tube. Centrifugation process was repeated with another 2 ml of sucrose cushion and 200 μl of top reserved fraction in fresh tubes, which served as a specificity and contamination control. Procedure for preparing input control samples and performing immunoblotting is as described above.

Newly synthesized actin-PLA labeling

Detection of newly synthesized proteins by PLA was carried out using anti-puromycin antibody in combination with protein-specific antibodies and detection using Duolink reagents (Sigma-Aldrich) according to the manufacturer's recommendations. Briefly, disassociated cortical neurons (DIV11) were treated with puromycin (10 μg/ml) for 20 min and fixed for 20 min. After three times washing with PBS, cells were permeabilized for 15 min with 0.5% Triton X-100 in PBS and blocked in 4% goat serum in PBS for 1 hour at 37°C. Cells were co-incubated with mouse anti-puromycin antibody (Kerafast Equation 0001, 1:100) and rabbit anti-actin antibody (catalog no. A2066, Sigma-Aldrich; 1:100) at 4°C overnight. PLA probes mouse PLA^{plus} and rabbit PLA^{minus} were used for the puro-actin PLA procedure as described previously (*45*, *46*), and a far-red fluorescence-labeled oligo (Duolink Detection Reagents FarRed) was used for detecting the newly synthesized actin protein.

After PLA labeling, cells were post-fixed in 4% paraformaldehyde at room temperature for 10 min and washed with PBS for detection of the Slack expression immunostaining with the primary antibody anti-Slack (1:500; Aves labs, custom) and secondary antibody Alexa Fluor 488 anti-chicken (1:500; Thermo Fisher Scientific, A-11039) as described previously (*78*). Images were acquired using a Leica SP5 confocal microscope with a ×100 magnification. *Z*-series stack confocal images were taken. All confocal images were processed with ImageJ. Actin/PLA puncta were counted on the soma and on neurites within 100 μm of the soma. If there were two or more closely spaced somata for which it was not possible to attribute specific neurites to a given soma, then the somatic puncta were counted separately and all of the associated neuritic puncta were counted and divided equally among the somata.

Statistics and data analysis

Data analysis, imaging processing, and graphing were performed using Microsoft Excel (Microsoft), MATLAB (MathWorks), and Prism (GraphPad). All data are expressed as means ± SEM. Statistical analysis included two-way/one-way repeated measures/ordinary analysis of variance (ANOVA) with post hoc comparisons and paired/unpaired Student's *t* test. Multiple comparisons using the Holm-Šídák method were performed where noted. The statistical test used for each experiment can be found in the corresponding figure legend and data S2. Throughout, $*P < 0.05$, $**P < 0.01$, and $***P < 0.001$. Exact *P* values can be found in data S2.

Supplementary Materials

The PDF file includes:

Figs. S1 and S2
Table S1
Legends for data S1 and S2

Other Supplementary Material for this manuscript includes the following:

Data S1 and S2

REFERENCES AND NOTES

1. A. Bhattacharjee, L. K. Kaczmarek, For K^+ channels, Na^+ is the new Ca^{2+}. *Trends Neurosci.* **28**, 422–428 (2005).
2. W. J. Joiner, M. D. Tang, L. Y. Wang, S. I. Dworetzky, C. G. Boissard, L. Gan, V. K. Gribkoff, L. K. Kaczmarek, Formation of intermediate-conductance calcium-activated potassium channels by interaction of Slack and Slo subunits. *Nat. Neurosci.* **1**, 462–469 (1998).
3. J. Wu, L. El-Hassar, D. Datta, M. Thomas, Y. Zhang, D. P. Jenkins, N. J. DeLuca, M. Chatterjee, V. K. Gribkoff, A. F. T. Arnsten, L. K. Kaczmarek, Interaction between HCN and slack channels regulates mPFC pyramidal cell excitability in working memory circuits. *Mol. Neurobiol.* **61**, 2430–2445 (2024).
4. A. Bhattacharjee, C. A. von Hehn, X. Mei, L. K. Kaczmarek, Localization of the Na^+–activated K^+ channel Slick in the rat central nervous system. *J. Comp. Neurol.* **484**, 80–92 (2005).
5. A. Bhattacharjee, L. Gan, L. K. Kaczmarek, Localization of the Slack potassium channel in the rat central nervous system. *J. Comp. Neurol.* **454**, 241–254 (2002).
6. A. Bhattacharjee, W. J. Joiner, M. Wu, Y. Yang, F. J. Sigworth, L. K. Kaczmarek, Slick (Slo2.1), a rapidly-gating sodium-activated potassium channel inhibited by ATP. *J. Neurosci.* **23**, 11681–11691 (2003).
7. G. Barcia, M. R. Fleming, A. Deligniere, V. R. Gazula, M. R. Brown, M. Langouet, H. Chen, J. Kronengold, A. Abhyankar, R. Cilio, P. Nitschke, A. Kaminska, N. Boddaert, J. L. Casanova, I. Desguerre, A. Munnich, O. Dulac, L. K. Kaczmarek, L. Colleaux, R. Nabbout, De novo gain-of-function KCNT1 channel mutations cause malignant migrating partial seizures of infancy. *Nat. Genet.* **44**, 1255–1259 (2012).
8. S. E. Heron, K. R. Smith, M. Bahlo, L. Nobili, E. Kahana, L. Licchetta, K. L. Oliver, A. Mazarib, Z. Afawi, A. Korczyn, G. Plazzi, S. Petrou, S. F. Berkovic, I. E. Scheffer, L.M. Dibbens, Missense mutations in the sodium-gated potassium channel gene KCNT1 cause severe autosomal dominant nocturnal frontal lobe epilepsy. *Nat. Genet.* **44**, 1188–1190 (2012).
9. H. C. Martin, G. E. Kim, A. T. Pagnamenta, Y. Murakami, G. L. Carvill, E. Meyer, R. R. Copley, A. Rimmer, G. Barcia, M. R. Fleming, J. Kronengold, M. R. Brown, K. A. Hudspith, J. Broxholme, A. Kanapin, J. B. Cazier, T. Kinoshita, R. Nabbout, W. G. S. Consortium, D. Bentley, G. McVean, S. Heavin, Z. Zaiwalla, T. McShane, H. C. Mefford, D. Shears, H. Stewart, M. A. Kurian, I. E. Scheffer, E. Blair, P. Donnelly, L. K. Kaczmarek, J. C. Taylor, Clinical whole-genome sequencing in severe early-onset epilepsy reveals new genes and improves molecular diagnosis. *Hum. Mol. Genet.* **23**, 3200–3211 (2014).
10. G. E. Kim, L. K. Kaczmarek, Emerging role of the KCNT1 Slack channel in intellectual disability. *Front. Cell. Neurosci.* **8**, 209 (2014).
11. M. R. Brown, J. Kronengold, V. R. Gazula, Y. Chen, J. G. Strumbos, F. J. Sigworth, D. Navaratnam, L. K. Kaczmarek, Fragile X mental retardation protein controls gating of the sodium-activated potassium channel Slack. *Nat. Neurosci.* **13**, 819–821 (2010).
12. Y. Zhang, M. R. Brown, C. Hyland, Y. Chen, J. Kronengold, M. R. Fleming, A. B. Kohn, L. L. Moroz, L. K. Kaczmarek, Regulation of neuronal excitability by interaction of fragile X mental retardation protein with slack potassium channels. *J. Neurosci.* **32**, 15318–15327 (2012).
13. X. Zhan, H. Asmara, N. Cheng, G. Sahu, E. Sanchez, F. X. Zhang, G. W. Zamponi, J. M. Rho, R. W. Turner, FMRP(1-297)-tat restores ion channel and synaptic function in a model of Fragile X syndrome. *Nat. Commun.* **11**, 2755 (2020).
14. P. Y. Deng, D. Carlin, Y. M. Oh, L. K. Myrick, S. T. Warren, V. Cavalli, V. A. Klyachko, Voltage-independent SK-channel dysfunction causes neuronal hyperexcitability in the hippocampus of Fmr1 knock-out mice. *J. Neurosci.* **39**, 28–43 (2019).
15. P. Y. Deng, V. A. Klyachko, Channelopathies in fragile X syndrome. *Nat. Rev. Neurosci.* **22**, 275–289 (2021).
16. P. Y. Deng, Z. Rotman, J. A. Blundon, Y. Cho, J. Cui, V. Cavalli, S. S. Zakharenko, V. A. Klyachko, FMRP regulates neurotransmitter release and synaptic information transmission by modulating action potential duration via BK channels. *Neuron* **77**, 696–711 (2013).
17. L. K. Myrick, P. Y. Deng, H. Hashimoto, Y. M. Oh, Y. Cho, M. J. Poidevin, J. A. Suhl, J. Visootsak, V. Cavalli, P. Jin, X. Cheng, S. T. Warren, V. A. Klyachko, Independent role for presynaptic FMRP revealed by an FMR1 missense mutation associated with intellectual disability and seizures. *Proc. Natl. Acad. Sci. U.S.A.* **112**, 949–956 (2015).
18. Y. M. Yang, J. Arsenault, A. Bah, M. Krzeminski, A. Fekete, O. Y. Chao, L. K. Pacey, A. Wang, J. Forman-Kay, D. R. Hampson, L. Y. Wang, Identification of a molecular locus for normalizing dysregulated GABA release from interneurons in the Fragile X brain. *Mol. Psychiatry* **25**, 2017–2035 (2020).
19. L. Ferron, M. Nieto-Rostro, J. S. Cassidy, A. C. Dolphin, Fragile X mental retardation protein controls synaptic vesicle exocytosis by modulating N-type calcium channel density. *Nat. Commun.* **5**, 3628 (2014).
20. R. J. Hagerman, L. W. Staley, R. O'Conner, K. Lugenbeel, D. Nelson, S. D. McLean, A. Taylor, Learning-disabled males with a fragile X CGG expansion in the upper premutation size range. *Pediatrics* **97**, 122–126 (1996).
21. O. Steward, E. M. Schuman, Protein synthesis at synaptic sites on dendrites. *Annu. Rev. Neurosci.* **24**, 299–325 (2001).
22. R. Lu, H. Wang, Z. Liang, L. Ku, T. O'donnell, W. Li, S. T. Warren, Y. Feng, The fragile X protein controls microtubule-associated protein 1B translation and microtubule stability in brain neuron development. *Proc. Natl. Acad. Sci. U.S.A.* **101**, 15201–15206 (2004).
23. F. Zalfa, M. Giorgi, B. Primerano, A. Moro, A. Di Penta, S. Reis, B. Oostra, C. Bagni, The fragile X syndrome protein FMRP associates with BC1 RNA and regulates the translation of specific mRNAs at synapses. *Cell* **112**, 317–327 (2003).
24. M. R. Fleming, M. R. Brown, J. Kronengold, Y. Zhang, D. P. Jenkins, G. Barcia, R. Nabbout, A. E. Bausch, P. Ruth, R. Lukowski, D. S. Navaratnam, L. K. Kaczmarek, Stimulation of Slack K(+) channels alters mass at the plasma membrane by triggering dissociation of a phosphatase-regulatory complex. *Cell Rep.* **16**, 2281–2288 (2016).

25. I. Napoli, V. Mercaldo, P. P. Boyl, B. Eleuteri, F. Zalfa, S. De Rubeis, D. Di Marino, E. Mohr, M. Massimi, M. Falconi, W. Witke, M. Costa-Mattioli, N. Sonenberg, T. Achsel, C. Bagni, The fragile X syndrome protein represses activity-dependent translation through CYFIP1, a new 4E-BP. *Cell* **134**, 1042–1054 (2008).
26. S. De Rubeis, C. Bagni, Fragile X mental retardation protein control of neuronal mRNA metabolism: Insights into mRNA stability. *Mol. Cell. Neurosci.* **43**, 43–50 (2010).
27. E. Santini, T. N. Huynh, F. Longo, S. Y. Koo, E. Mojica, L. D'Andrea, C. Bagni, E. Klann, Reducing eIF4E-eIF4G interactions restores the balance between protein synthesis and actin dynamics in fragile X syndrome model mice. *Sci. Signal.* **10**, eaan0665 (2017).
28. D. Panja, J. W. Kenney, L. D'Andrea, F. Zalfa, A. Vedeler, K. Wibrand, R. Fukunaga, C. Bagni, C. G. Proud, C. R. Bramham, Two-stage translational control of dentate gyrus LTP consolidation is mediated by sustained BDNF-TrkB signaling to MNK. *Cell Rep.* **9**, 1430–1445 (2014).
29. S. Patil, K. Chalkiadaki, T. F. Mergiya, K. Krimbacher, I. S. Amorim, S. Akerkar, C. G. Gkogkas, C. R. Bramham, eIF4E phosphorylation recruits β-catenin to mRNA cap and promotes Wnt pathway translation in dentate gyrus LTP maintenance. *iScience* **26**, 106649 (2023).
30. J. C. Darnell, S. J. Van Driesche, C. Zhang, K. Y. Hung, A. Mele, C. E. Fraser, E. F. Stone, C. Chen, J. J. Fak, S. W. Chi, D. D. Licatalosi, J. D. Richter, R. B. Darnell, FMRP stalls ribosomal translocation on mRNAs linked to synaptic function and autism. *Cell* **146**, 247–261 (2011).
31. A. R. Buxbaum, B. Wu, R. H. Singer, Single β-actin mRNA detection in neurons reveals a mechanism for regulating its translatability. *Science* **343**, 419–422 (2014).
32. D. M. Chudakov, S. Lukyanov, K. A. Lukyanov, Tracking intracellular protein movements using photoswitchable fluorescent proteins PS-CFP2 and Dendra2. *Nat. Protoc.* **2**, 2024–2032 (2007).
33. D. M. Chudakov, S. Lukyanov, K. A. Lukyanov, Using photoactivatable fluorescent protein Dendra2 to track protein movement. *Biotechniques* **42**, 553–563 (2007).
34. G. E. Kim, J. Kronengold, G. Barcia, I. H. Quraishi, H. C. Martin, E. Blair, J. C. Taylor, O. Dulac, L. Colleaux, R. Nabbout, L. K. Kaczmarek, Human slack potassium channel mutations increase positive cooperativity between individual channels. *Cell Rep.* **9**, 1661–1672 (2014).
35. I. H. Quraishi, M. R. Mercier, H. McClure, R. L. Couture, M. L. Schwartz, R. Lukowski, P. Ruth, L. K. Kaczmarek, Impaired motor skill learning and altered seizure susceptibility in mice with loss or gain of function of the Kcnt1 gene encoding Slack (KNa1.1) Na^+-activated K^+ channels. *Sci. Rep.* **10**, 3213 (2020).
36. E. Miyamoto-Sato, N. Nemoto, K. Kobayashi, H. Yanagawa, Specific bonding of puromycin to full-length protein at the C-terminus. *Nucleic Acids Res.* **28**, 1176–1182 (2000).
37. K. Welshhans, G. J. Bassell, Netrin-1-induced local β-actin synthesis and growth cone guidance requires zipcode binding protein 1. *J. Neurosci.* **31**, 9800–9813 (2011).
38. S. A. Swanger, Y. A. He, J. D. Richter, G. J. Bassell, Dendritic GluN2A synthesis mediates activity-induced NMDA receptor insertion. *J. Neurosci.* **33**, 8898–8908 (2013).
39. Y. I. Zilberter, C. F. Starmer, A. O. Grant, Open Na+ channel blockade: Multiple rest states revealed by channel interactions with disopyramide and quinidine. *Am. J. Physiol.* **266**, H2007–H2017 (1994).
40. S. J. Kehl, Quinidine-induced inhibition of the fast transient outward K+ current in rat melanotrophs. *Br. J. Pharmacol.* **103**, 1807–1813 (1991).
41. B. Yang, V. K. Gribkoff, J. Pan, V. Damagnez, S. I. Dworetzky, C. G. Boissard, A. Bhattacharjee, Y. Yan, F. J. Sigworth, L. K. Kaczmarek, Pharmacological activation and inhibition of Slack (Slo2.2) channels. *Neuropharmacology* **51**, 896–906 (2006).
42. K. Lee, I. C. Rowe, M. L. Ashford, NS 1619 activates BKCa channel activity in rat cortical neurones. *Eur. J. Pharmacol.* **280**, 215–219 (1995).
43. A. E. Bausch, R. Dieter, Y. Nann, M. Hausmann, N. Meyerdierks, L. K. Kaczmarek, P. Ruth, R. Lukowski, The sodium-activated potassium channel Slack is required for optimal cognitive flexibility in mice. *Learn. Mem.* **22**, 323–335 (2015).
44. L. Matt, T. Pham, D. Skrabak, F. Hoffmann, P. Eckert, J. Yin, M. Gisevius, R. Ehinger, A. Bausch, M. Ueffing, K. Boldt, P. Ruth, R. Lukowski, The Na^+-activated K^+ channel Slack contributes to synaptic development and plasticity. *Cell. Mol. Life Sci.* **78**, 7569–7587 (2021).
45. S. Sambandan, G. Akbalik, L. Kochen, J. Rinne, J. Kahlstatt, C. Glock, G. Tushev, B. Alvarez-Castelao, A. Heckel, E. M. Schuman, Activity-dependent spatially localized miRNA maturation in neuronal dendrites. *Science* **355**, 634–637 (2017).
46. S. tom Dieck, L. Kochen, C. Hanus, M. Heumuller, I. Bartnik, B. Nassim-Assir, K. Merk, T. Mosler, S. Garg, S. Bunse, D. A. Tirrell, E. M. Schuman, Direct visualization of newly synthesized target proteins in situ. *Nat. Methods* **12**, 411–414 (2015).
47. T. J. Younts, H. R. Monday, B. Dudok, M. E. Klein, B. A. Jordan, I. Katona, P. E. Castillo, Presynaptic protein synthesis is required for long-term plasticity of GABA release. *Neuron* **92**, 479–492 (2016).
48. H. R. Monday, S. C. Kharod, Y. J. Yoon, R. H. Singer, P. E. Castillo, Presynaptic FMRP and local protein synthesis support structural and functional plasticity of glutamatergic axon terminals. *Neuron* **110**, 2588–2606.e6 (2022).
49. S. B. Baltaci, R. Mogulkoc, A. K. Baltaci, Molecular mechanisms of early and late LTP. *Neurochem. Res.* **44**, 281–296 (2019).
50. D. H. Ebert, M. E. Greenberg, Activity-dependent neuronal signalling and autism spectrum disorder. *Nature* **493**, 327–337 (2013).
51. M. W. Waung, K. M. Huber, Protein translation in synaptic plasticity: mGluR-LTD, Fragile X. *Curr. Opin. Neurobiol.* **19**, 319–326 (2009).
52. R. Gray, D. Johnston, Sodium sensitivity of K_{Na} channels in mouse CA1 neurons. *J. Neurophysiol.* **125**, 1690–1697 (2021).
53. N. J. McGlincy, N. T. Ingolia, Transcriptome-wide measurement of translation by ribosome profiling. *Methods* **126**, 112–129 (2017).
54. S. Ceman, W. T. O'Donnell, M. Reed, S. Patton, J. Pohl, S. T. Warren, Phosphorylation influences the translation state of FMRP-associated polyribosomes. *Hum. Mol. Genet.* **12**, 3295–3305 (2003).
55. B. Tsang, J. Arsenault, R. M. Vernon, H. Lin, N. Sonenberg, L. Y. Wang, A. Bah, J. D. Forman-Kay, Phosphoregulated FMRP phase separation models activity-dependent translation through bidirectional control of mRNA granule formation. *Proc. Natl. Acad. Sci. U.S.A.* **116**, 4218–4227 (2019).
56. B. Biton, S. Sethuramanujam, K. E. Picchione, A. Bhattacharjee, N. Khessibi, F. Chesney, C. Lanneau, O. Curet, P. Avenet, The antipsychotic drug loxapine is an opener of the sodium-activated potassium channel slack (Slo2.2). *J. Pharmacol. Exp. Ther.* **340**, 706–715 (2012).
57. R. Goering, L. I. Hudish, B. B. Guzman, N. Raj, G. J. Bassell, H. A. Russ, D. Dominguez, J. M. Taliaferro, FMRP promotes RNA localization to neuronal projections through interactions between its RGG domain and G-quadruplex RNA sequences. *eLife* **9**, e52621 (2020).
58. P. Licznerski, H. A. Park, H. Rolyan, R. Chen, N. Mnatsakanyan, P. Miranda, M. Graham, J. Wu, N. Cruz-Reyes, N. Mehta, S. Sohail, J. Salcedo, E. Song, C. Effman, S. Effman, L. Brandao, G. N. Xu, A. Braker, V. K. Gribkoff, R. J. Levy, E. A. Jonas, ATP synthase c-subunit leak causes aberrant cellular metabolism in fragile X syndrome. *Cell* **182**, 1170–1185.e9 (2020).
59. J. D. Richter, G. J. Bassell, E. Klann, Dysregulation and restoration of translational homeostasis in fragile X syndrome. *Nat. Rev. Neurosci.* **16**, 595–605 (2015).
60. A. J. Verkerk, M. Pieretti, J. S. Sutcliffe, Y. H. Fu, D. P. Kuhl, A. Pizzuti, O. Reiner, S. Richards, M. F. Victoria, F. P. Zhang, B. E. Eussen, G. J. B. van Ommen, L. A. J. Blonden, G. J. Riggins, J. L. Chastain, C. B. Kunst, H. Galjaard, C. Thomas Caskey, D. L. Nelson, B. A. Oostra, S. T. Warren, Identification of a gene (FMR-1) containing a CGG repeat coincident with a breakpoint cluster region exhibiting length variation in fragile X syndrome. *Cell* **65**, 905–914 (1991).
61. J. D. Richter, X. Zhao, The molecular biology of FMRP: New insights into fragile X syndrome. *Nat. Rev. Neurosci.* **22**, 209–222 (2021).
62. S. S. Seo, S. R. Louros, N. Anstey, M. A. Gonzalez-Lozano, C. B. Harper, N. C. Verity, O. Dando, S. R. Thomson, J. C. Darnell, P. C. Kind, K. W. Li, E. K. Osterweil, Excess ribosomal protein production unbalances translation in a model of fragile X syndrome. *Nat. Commun.* **13**, 3236 (2022).
63. C. R. Hale, K. Sawicka, K. Mora, J. J. Fak, J. J. Kang, P. Cutrim, K. Cialowicz, T. S. Carroll, R. B. Darnell, FMRP regulates mRNAs encoding distinct functions in the cell body and dendrites of CA1 pyramidal neurons. *eLife* **10**, e71892 (2021).
64. C. T. Ashley Jr., K. D. Wilkinson, D. Reines, S. T. Warren, FMR1 protein: Conserved RNP family domains and selective RNA binding. *Science* **262**, 563–566 (1993).
65. V. Brown, P. Jin, S. Ceman, J. C. Darnell, W. T. O'Donnell, S. A. Tenenbaum, X. Jin, Y. Feng, K. D. Wilkinson, J. D. Keene, R. B. Darnell, S. T. Warren, Microarray identification of FMRP-associated brain mRNAs and altered mRNA translational profiles in fragile X syndrome. *Cell* **107**, 477–487 (2001).
66. M. Genheden, J. W. Kenney, H. E. Johnston, A. Manousopoulou, S. D. Garbis, C. G. Proud, BDNF stimulation of protein synthesis in cortical neurons requires the MAP kinase-interacting kinase MNK1. *J. Neurosci.* **35**, 972–984 (2015).
67. J. Wu, I. H. Quraishi, Y. Zhang, M. Bromwich, L. K. Kaczmarek, Disease-causing Slack potassium channel mutations produce opposite effects on excitability of excitatory and inhibitory neurons. *Cell Rep.* **43**, 113904 (2024).
68. F. Picard, P. Makrythanasis, V. Navarro, S. Ishida, J. de Bellescize, D. Ville, S. Weckhuysen, E. Fosselle, A. Suls, P. De Jonghe, M. Vasselon Raina, G. Lesca, C. Depienne, I. An-Gourfinkel, M. Vlaicu, M. Baulac, E. Mundwiller, P. Couarch, R. Combi, L. Ferini-Strambi, A. Gambardella, S. E. Antonarakis, E. Leguern, O. Steinlein, S. Baulac, DEPDC5 mutations in families presenting as autosomal dominant nocturnal frontal lobe epilepsy. *Neurology* **82**, 2101–2106 (2014).
69. R. Combi, L. Dalpra, M. L. Tenchini, L. Ferini-Strambi, Autosomal dominant nocturnal frontal lobe epilepsy--a critical overview. *J. Neurol.* **251**, 923–934 (2004).
70. H. Kurahashi, S. Hirose, *GeneReviews*, M. P. Adam, J. Feldman, G. M Mirzaa, R. A Pagon, S. E Wallace, A. Amemiya, Eds. (University of Washington, 1993).
71. E. Raimondeau, J. C. Bufton, C. Schaffitzel, New insights into the interplay between the translation machinery and nonsense-mediated mRNA decay factors. *Biochem. Soc. Trans.* **46**, 503–512 (2018).
72. L. A. Jolly, C. C. Homan, R. Jacob, S. Barry, J. Gecz, The UPF3B gene, implicated in intellectual disability, autism, ADHD and childhood onset schizophrenia regulates neural progenitor cell behaviour and neuronal outgrowth. *Hum. Mol. Genet.* **22**, 4673–4687 (2013).
73. G. Neu-Yilik, E. Raimondeau, B. Eliseev, L. Yeramala, B. Amthor, A. Deniaud, K. Huard, K. Kerschgens, M. W. Hentze, C. Schaffitzel, A. E. Kulozik, Dual function of UPF3B in early and late translation termination. *EMBO J.* **36**, 2968–2986 (2017).

74. T. J. Malone, L. K. Kaczmarek, The role of altered translation in intellectual disability and epilepsy. *Prog. Neurobiol.* **213**, 102267 (2022).
75. H. Chen, J. Kronengold, Y. Yan, V. R. Gazula, M. R. Brown, L. Ma, G. Ferreira, Y. Yang, A. Bhattacharjee, F. J. Sigworth, L. Salkoff, L. K. Kaczmarek, The N-terminal domain of Slack determines the formation and trafficking of Slick/Slack heteromeric sodium-activated potassium channels. *J. Neurosci.* **29**, 5654–5665 (2009).
76. R. Lu, A. E. Bausch, W. Kallenborn-Gerhardt, C. Stoetzer, N. Debruin, P. Ruth, G. Geisslinger, A. Leffler, R. Lukowski, A. Schmidtko, Slack channels expressed in sensory neurons control neuropathic pain in mice. *J. Neurosci.* **35**, 1125–1135 (2015).
77. H. A. Park, P. Licznerski, N. Mnatsakanyan, Y. Niu, S. Sacchetti, J. Wu, B. M. Polster, K. N. Alavian, E. A. Jonas, Inhibition of Bcl-xL prevents pro-death actions of DeltaN-Bcl-xL at the mitochondrial inner membrane during glutamate excitotoxicity. *Cell Death Differ.* **24**, 1963–1974 (2017).
78. S. R. Ali, T. J. Malone, Y. Zhang, M. Prechova, L. K. Kaczmarek, Phactr1 regulates Slack (KCNT1) channels via protein phosphatase 1 (PP1). *FASEB J.* **34**, 1591–1601 (2020).

Acknowledgments:
Funding: This work was supported by the National Institutes of Health (NIH), grants NS102239 and DC01919 (L.K.K.), NS112706 (E.A.J.), and GM007324 (T.J.M.); by CTSA grant number UL1 TR001863 (J.W.) from the National Center for Advancing Translational Sciences (NCATS), a component of the NIH; and by a FRAXA grant (Y.Z.). **Author contributions:** Conceptualization: T.J.M., J.W., and L.K.K. Methodology: T.J.M., J.W., Y.Z., P.L., E.A.J., and L.K.K. Software: T.J.M., S.N., and M.P. Investigation: T.J.M., J.W., Y.Z., P.L., R.C., S.N., and M.P. Data curation: T.J.M., J.W., Y.Z., M.P., and L.K.K. Validation: T.J.M., J.W., Y.Z., S.N., and M.P. Formal analysis: T.J.M., J.W., Y.Z., P.L., S.N., M.P., and L.K.K. Visualization: T.J.M., J.W., Y.Z., M.P., and L.K.K. Resources: J.W., Y.Z., M.P., E.A.J., and L.K.K. Writing—original draft: T.J.M., J.W., and L.K.K. Writing—review and editing: T.J.M., J.W., Y.Z., M.P., E.A.J., and L.K.K. Funding acquisition: T.J.M., J.W., Y.Z., E.A.J., and L.K.K. Project administration: L.K.K. Supervision: E.A.J. and L.K.K. **Competing interests:** The authors declare that they have no competing interests. **Data and materials availability:** The *Slack*$^{+/R455H}$ mouse line is available from the corresponding author, L.K.K. (leonard.kaczmarek@yale.edu), with a completed material transfer agreement. All data needed to evaluate the conclusions in the paper are present in the paper and/or the Supplementary Materials. All custom code used for semiautomated FRAP is available at DOI: 10.5281/zenodo.14933585.

Submitted 13 December 2024
Accepted 23 April 2025
Published 28 May 2025
10.1126/sciadv.adv3140